Published in final edited form as:
IEEE Trans Instrum Meas. 2020 June ; 69(6): 3882–3895. doi:10.1109/tim.2019.2938131.

Application-Adaptable Chipless RFID Tag: Design Methodology, Metrics, and Measurements

Katelyn R. Brinker [Student member, IEEE], **Marshall Vaccaro**, **Reza Zoughi [Fellow, IEEE]**
Applied Microwave Nondestructive Testing Laboratory at the Missouri University of Science and Technology, Rolla, MO 65401 USA.

Abstract

The field of chipless RFID is growing due to the cost effectiveness, simplicity, and versatility of the technology. Typically, chipless RFID tags utilize a single type of resonator in their design and are designed for a singular application. These design practices are limiting both in terms of versatility and practicality. This work builds on previous work and proposes a new application-adaptable tag design methodology. This methodology revolves around the use of combinations of multiple types of resonators in backscatter-based frequency-coded tag designs for the purpose of enhancing versatility and utility of chipless RFID technology. From this novel design methodology, an original tag design presented previously that achieves a high bit density of 27.54 bits/cm^2 is further analyzed and optimized for two applications. Furthermore, this paper presents a method for associating tag response characteristics to tag geometry and develops new tag metrics that can be used to more effectively compare the merits of sensing-based tags. Measurements of manufactured tags are also presented, and associated measurement challenges are discussed.

Index Terms

bit density; Chipless RFID; spiral resonators; application adaptability

I. Introduction

As chipless RFID technology has developed, so has its realm of applications. Chipless RFID is a subset of the RFID field in which the tags neither have a power source nor an IC. Instead, the “stored” information is inherent to the geometrical structure of the tag. For frequency coded tags, the structure produces a specific spectral response (e.g., radar cross section (RCS) or complex reflection coefficient (S_{11}) vs. frequency) to which a binary code is assigned. This binary code can be assigned in a variety of ways depending on the application and tag design specifications [1, 2]. Typical applications of chipless RFID are identification and sensing [2, 3]. For identification-based tags, a binary code is assigned to the tag response and it is desirable for this code to be as long as possible so that more

katelyn.brinker@umsystem.edu .

IDs can be generated and assigned. At the same time, it is desirable for these tags to be space-efficient (i.e., have a small form-factor) so that they can have practical utilities. Bit density, defined as the number of bits in the binary code per centimeter squared of tag area, is a metric often used for ID-based tags to describe how well a tag balances the need for code length and space efficiency [3]. For sensing-based tags, the trend has been to utilize changes of a single resonance in the tag response to sense a physical parameter such as temperature, strain, or humidity [4–6]. Since only a single resonance is used, typically a binary code is not assigned to the responses of these tags. Therefore, measurand sensitivity, which is how significantly the measured parameter changes as a function of the parameter being monitored (e.g., what voltage change occurs as a function of temperature for a temperature sensor), is sometimes used for sensing-based tags.

A common feature between ID- and sensing-based tags is that they are typically designed with a specific application in mind. In a few cases, a sensing bit is added to an ID-based tag, or ID bits are added to a sensing tag. However, in both of these cases this is done to enhance tag performance for the original application [7, 8]. This combination of application specificity and lack of resonator diversity are limiting in terms of versatility and practicality. For example, if there exists a certain requirement in the size (area) of a tag, then a design can only contain a limited number of a particular type of a resonator before the area is full. Therefore, the tag can only achieve a limited bit density. To mitigate this, the tag can be designed to operate at higher frequencies, at which smaller resonators can be incorporated. However, with this approach the design reaches a point where the resonators become very small and difficult or costly to manufacture, while also the tag characteristic response becomes more difficult to measure. This approach to tag design causes customizability of the response with a singular type of resonator and a specified tag area is limited. Thus, the applications for which the tag can be used are limited. Alternatively, by combining multiple types of resonators, greater response variation, higher bit densities, and in turn greater application diversity (i.e., use in multiple applications, such as both ID and sensing applications) can be achieved. These advantages will be illustrated throughout this paper.

Another commonality between ID- and sensing-based chipless RFID tags, is measurement difficulty. In many cases, the RCS of the tag is measured. This is done because RCS is distance independent while S_{11} is distance dependent. However, RCS measurement can be difficult to make and often requires the use of calibration targets, which makes it difficult to measure the RCS outside a controlled laboratory setting [9–11]. Another measurement challenge in the area of chipless RFID is orientation sensitivity [12, 13]. These issues then lead to limited read range and difficulty localizing tags. To overcome these issues, some different measurement methods such as using an ultra-wideband (UWB) pulse for interrogation and different reader antennas have been proposed [14, 15]. Post processing techniques, to extract tag signatures from measured responses, have also been proposed to help overcome these measurement challenges [16, 17]. Another approach has been to design tags differently to increase the tag response signal in relation to the response of the background (i.e., environment). Primary examples of these different types of tags are depolarizing tags and harmonic tags [18, 19]. Additional solutions have been proposed in the area of traditional RFID. Some of these solutions include using phase and amplitude information with specialized algorithms to perform 2d tag localization, characterizing

multipath to reduce RF distance error, and metrically characterizing the effect of the environment on the RFID system [20–22]. These methods could also potentially be applied to the area of chipless RFID to help solve the previously mentioned measurement issues. Overall, though, there is still more work to be done to understand these measurement challenges, how they affect chipless RFID sensing capabilities, and how to overcome them. In this work, we explore these measurement challenges, especially the effects of orientation and distance dependence.

This paper discusses a novel application-adaptable tag *design methodology* which is founded on methodically combining characteristic responses of serval different resonators. A preliminary tag design that achieves an extremely high bit density employing this approach was previously presented in [23] and is analyzed in detail here. Additionally, results of optimization for different applications using the principles of the design methodology are presented. Finally, utilizing simulation tools to analyze tag responses, common and new tag metrics, and measurement results of the designed tag are discussed. Together, these methodologies, designs, and experiments represent a new way to approach chipless RFID tag design, while also discussing the challenges and limitations of the technology especially in terms of measurement. This work serves as a technical extension of [23] and uses some content in sections III to VII from the thesis [24] with permission.

II. Application-Adaptable Tag Design Methodology

Combining multiple types of resonators into one tag, provides greater versatility, both in terms of creating more unique binary codes and optimizing for different applications. However, in order to do so properly, it is necessary to understand how the resonant frequencies of tag elements (i.e., resonators) react to changes in their own basic geometries and the manner by which these resonant tag elements interact with each other. Only in this way can the tag response can be designed and developed in a controlled and predictable manner. Design guidelines, such as design curves, equivalent circuits, and mathematical models of the resonant behavior of these tag elements, become necessary and extremely beneficial for this process. They provide the tag designer with the necessary guidelines for designing tags that meet certain requirements, all without relying on trial-and-error simulation or retrofitting a tag design to a new application for which it may not be well-suited. Some design guidelines have been reported for singular resonators, but they often do not describe the interaction between multiple elements of the same resonator type or of multiple elements of different resonator types [25, 26]. Additionally, some of the design guidelines generated for microwave filter applications can be applied to chipless RFID tag design [27].

Besides understanding how tag elements operate and interact, it is necessary to understand the effect of the tag environment on this operation and these interactions. If the tag does not have a ground plane, the material the tag is attached to can have a large impact on the response of the tag. It has been shown that it is beneficial for a tag to have a ground plane if it is going to be pasted on an object since this will reduce the effect the object has on the response of the tag [7]. However, manufacturing a tag with a ground plane is not very conducive to inkjet printing, as many printing papers only have ink adhesion coatings

on one side (i.e., one can only print on one side of the paper). Despite these limitations, inkjet printability is still considered an important advantageous feature in tag design as this facilitates ease of deployment by way of being capable of being manufactured by a low-cost and quick method [3, 28].

Another important situation to consider is when a tag, without a ground plane, is placed in front of an electrically conducting surface (i.e., metal). In this situation, the conducting surface acts like a ground plane to the tag if the tag is sufficiently close it, and changes the tag response significantly. For example, the intended slot resonators may have their conductor features act as ring resonators causing different resonances in the frequency response. This is illustrated in Fig. 1 where the responses of a tag with and without a ground plane are compared. As can be seen from Fig. 1b, the response is significantly different for when the tag has a ground plane versus when it does not. If the conducting surface is large enough compared to the tag, the conducting surface creates an image theory situation whereby the tag overall response becomes a combination of itself and its image.

Other environmental factors like temperature and humidity also need to be taken into consideration when determining how to manufacture a tag. As previously mentioned, inkjet-printing is a very popular manufacturing method for chipless RFID. A popular substrate to print on is Mitsubishi paper. However, this paper is sensitive to humidity so if the tag were would change [6]. Consequently, it is necessary to have a complete understanding of the effects on tag response due to the environment in which the tag is intended to be placed.

By combining this understanding of environmental concerns with that of how tag elements operate and interact, tags can be effectively engineered to meet certain requirements and can easily be adapted to fit new applications. This understanding allows, for example, for a tag with a ground plane to be quickly modified to not have a ground plane so that it could more easily be manufactured via inkjet printing. In this sense, the tags become application-adaptable.

These practices can be summarized in a three step tag design methodology:

1. Define tag requirements: size, bit density, manufacturing method, understand current application and possible future applications.
2. Select resonators and resonator combinations that satisfy these requirements.
3. Utilize the design guidelines to purposefully modify the resonator geometries to create a desired tag response.

III. Tag Design

In this section, the design of a tag that was preliminarily discussed in [23] is presented in the context of the presented design methodology. In doing so, the design considerations not previously discussed, such as the spiral resonator dependency on the ring resonators and the response dependency on the location and orientation of spiral resonators, are demonstrated. Furthermore, justification for the dimensions and types of resonators used are provided, which is not frequently done in the chipless RFID field. An example of a case where this

is done is the work in [29]. This tag, which was initially designed and simulated in CST Microwave Studio®, consists of a ground plane backed TLX-9 substrate disk (ε_r=2.5 and tanδ=0.0019) with a diameter of 0.68 cm. Different types of resonators, are combined to create a spectral signature that lends itself to a high bit density tag design. By adding and removing resonators and resonator types, the response can be modified to adapt this tag for various applications. In its most basic configuration, this tag utilizes ring resonator and circular patch antenna. Spiral resonators can then be added to create responses with more notches, as initially discussed in [23].

The most basic form of this tag design and its RCS vs. frequency response are shown in Fig. 2. The RCS response was generated from a simulation in CST Microwave Studio®, in which a linearly-polarized plane-wave excitation was used in a monostatic radar configuration to illuminate the tag and a RCS probe was used to measure the response. The direction of the polarization is indicated in Fig. 2a. The frequency range of 18–35 GHz was chosen since it allowed the tag to be small and minimally invasive (if used for embedded sensing applications).

The tag response in Fig. 2b shows two notches as a function of frequency, namely: one at ~21 GHz which is associated with the ring resonator element and the second at ~34 GHz which is associated with the circular patch in the center. These notches indicate or set the *start* and *stop* bits for the binary code that will be associated with this tag when the tag is loaded with spiral resonators. This is especially useful when embedding such a tag in a material for characterizing its properties. The reason for this is that in materials characterization applications the response is expected to shift down in frequency, compress, and distort as a function of the material properties. Thus, having distinct start and stop response features can help identify which parts of the binary code in the overall response are due to the tag and which parts are due to the environment [30]. This is illustrated further in Section IV.

In designing the spiral resonators, first the top spiral (see Fig. 3) was designed to have a resonant frequency close to that of the ring resonator. The resonant frequency of a spiral resonator is related to the effective inductance and capacitance of the element (i.e., the longer the spiral is, the higher its effective inductance and capacitance and thus the lower its resonant frequency) [31]. This principle, along with design guidelines generated for using spiral resonators in microwave filters in [27], were applied to modify the spiral geometry in a purposeful manner to achieve the desired response characteristics. However, the design guidelines in [27] could not be directly applied since their design utilized a different feeding mechanism. Additionally, the resonators presented in these guidelines in [27] operated at a lower frequency range and were not used in such a way that orientation and location relative to another element and the interrogation polarization were of any concern. The first spiral resonator element that was designed is shown in Fig. 3. This element has a resonance frequency of 18.5 GHz when it is the only spiral element present. When other spiral elements are added, the interaction between them causes this first spiral resonance to shift between those resonances associated with the ring and the circular patch. In general there are three design considerations to take into account when it comes to integrating spiral resonators with a ring resonator:

1. The dependency of the spiral resonators on the ring resonator.
2. The effect of spiral orientation in relation to the reader polarization.
3. The effect of spiral location in relation to the reader polarization.

These three design considerations are detailed further below.

For this tag design, the circular patch can be removed from the tag and the ring resonator still provides its notch in the response. However, the ring resonator cannot be removed if the spiral resonators are going to be used in the tag, since the ring is needed to interact with the spirals. This dependency between the ring resonator and spiral resonators is considered a constraint of this tag design. This design constraint is illustrated in Figs. 3 and 4. Fig. 3 gives the schematics of the three different configurations examined to illustrate this point, and Fig. 4 shows the respective tag responses. As previously described, the ring still contributes a notch to the response when the patch is removed. However, the notch is slightly shifted in frequency without the patch, indicating the absence of the interaction between the two. For configurations in Figs. 3a and 3b, there is a resonance associated with the spiral at 18.5 GHz. For the configuration in Fig. 3c, there is still a notch in the response associated with the patch, but not one associated with the spiral. This is due to a lack of interaction between the patch and the spiral at 18.5 GHz which is indicated in the surface current density simulation in Fig. 5. Fig. 5 shows that there is not a high concentration of surface current on the circular patch at 18.5 GHz where the spiral should be resonating. In contrast, at 35 GHz where the patch would normally resonate there is a high concentration of surface current density on the patch but not on the spiral. Overall, these results shown in Figs. 4 and 5 indicate that the ring resonator is required for the spiral resonator elements to operate properly.

The other design considerations to be cognizant of include the orientation and location of the spiral resonators with respect to the polarization of the interrogating wave. In this tag design, rotating a spiral about its center at a specific location around the ring yields different responses. Likewise, moving the spiral to different locations around the ring results in different responses. Fig. 6 shows the effect of spiral orientation on tag response, while Figs. 7 and 8 show the location of spiral around the ring element and its effect on the tag response, respectively. For both of these figures, the spiral at the top position (Position 1) is rotated or relocated around the ring resonator in the tag.

Fig. 6 shows that each of the four orientations produces a different response, which could lead to different binary codes associated with the response depending on the coding method used. Fig. 8 shows the three different responses that occur as the spiral element is moved around the ring resonator element. These differences in response as a function of orientation and location can be attributed to differences in how the resonator interacts with the interrogating wave. In all of these cases, the tag is interrogated with a linearly polarized wave with the electric field along the x-axis (see Fig. 2a). These response dependencies can make it more challenging to understand how changes in element geometry affect the response. However, they can also be utilized to create greater response diversity. Additionally, this spatial sensitivity may be exploited to perform rotation sensing [32]. With this knowledge of the location and orientation dependency of the spiral element class, the

spiral elements of the tag were designed so that each spiral would contribute one notch to the response.

Spirals designed after the one at location 1 were designed one at a time to have higher resonant frequencies in order to add notches to the frequency range between the ring and the patch resonant frequencies. As part of this iterative design strategy, the four spirals seen in the four spiral tag configuration in Fig. 9a were designed so that the tag could operate primarily in K-band (18 – 26.5 GHz) and so each spiral would contribute a notch to the response. In achieving this, some of the spirals had to be rotated to different orientations to overcome destructive interference among response characteristics associated with different tag features.

In moving to the 8-spiral configuration, shown in Fig. 9b, the additional four spirals were designed to have resonant frequencies between those of the original four spirals and the start and stop bits, and to add four more notches to the response. The responses of both configurations shown in Fig. 9 are presented in Fig. 10. As can be seen, adding four additional spirals affects the magnitude of the notches and the locations of the notches present in the 4-spiral configuration response. This is due to coupling between the spirals. However, the locations of the start and stop bits remain the same. The 8-spiral configuration achieves a higher bit density than the 4-spiral configuration because there are four more notches in the RCS vs. frequency response, as expected. These two configuration were featured in [23].

Based on a spatial analysis, up to 12 spirals could potentially be placed around the ring resonator to further increase the bit density of the tag. However, doing so increases the complexity of the design process. In order to focus on application-adaptability and chipless RFID metrics and measurement challenges, the 8-spiral tag is utilized for the remainder of this work. Section VI discusses tag metrics and shows how the achieved high bit density compares to that of other tags.

The design methodology presented in Section II can be summarized in the context of this tag, as follows:

1. Requirements identification:
    - **a.** Operate at K-band or higher to allow for a small profile tag,
    - **b.** Have an extremely high bit density and be able to scale the bit density to fit the application (i.e., be able to easily have fewer notches in the response for non-identification applications like embedded materials characterization).
    - **c.** Be able to manufacture the tag as a PCB and utilize the tag for both identification and materials characterization applications.
2. Resonator selection:
    - **a.** The circular patch and ring resonator provide for stable start and stop bits, which are desirable for embedded materials characterization applications.

b. The orientation and location sensitivity of the spirals allow for greater response diversity, which is desirable for identification applications.

c. Spiral resonators are space efficient allowing for greater bit density.

3. Design guideline utilization to combine resonators in a purposeful manner:

a. Design guidelines from [24] along with an understanding of location and orientation sensitivity were developed and utilized for this tag.

b. Surface current simulations were used to understand the relationship between tag features (see Fig. 5 and Section V).

c. Spirals were designed iteratively with increasing notch frequency.

d. The tag was then adapted and tested in the context of different applications, which is shown in Section IV.

In further improving the practicality of this tag by achieving a balance between manufacturability and cost, a lower frequency version was designed, which is shown with its response in Fig. 11. Being larger (diameter of 1.36 cm), this version of the tag could potentially be inkjet-printed in two separate layers as it would be within the manufacturing tolerances of a typical desktop inkjet printer or easily fabricated by a PCB manufacturer [28]. This version of the spiral tag also utilizes a detuning strategy, featured in [8], to make the response more robust to the removal of spirals which is useful for ID applications. In doing this, spirals with adjacent resonant frequencies are not placed next to each other around the ring resonator. This decreases the mutual coupling between the spiral resonators and allows the response to be more robust to resonator removal. In other words, when one spiral is removed from the tag structure, the response characteristics associated with the other tag elements remain relatively unchanged. Section VII shows the measurement of this version of the tag.

IV. Tag Application Suitability

The 8-spiral tag is well suited for embedded materials characterization applications due to the numerous notches in its response that allow for 3 different sensing approaches to be used, and could be used for ID applications. To further illustrate this, the 8-sprial tag from Fig. 9b was simulated as an embedded sensor in materials with different relative dielectric constants (ε_r) (i.e., different permittivities (ε_r') and loss factors (ε_r")), as shown in Fig. 12. As was illustrated in [30], when a chipless RFID tag is embedded in a material, the response of the tag shifts, compresses, and distorts as a function of the material properties in which it is embedded. This can be explained by the tag appearing electrically larger in a material that has a relative permittivity greater than one. The effect of embedding material's permittivity on the tag response is shown in Fig. 12b. If a binary code were to be assigned to the response, this code would change as a function of the material the tag is embedded in. Furthermore, the lossier the material, the greater the distortion in its response, changing the code associated with the tag. This effect is shown in Fig. 12c. This method of utilizing the code associated with a tag response that consists of multiple notches to determine material characteristics, provides more reliability when it comes to practical use since it does not rely

on the accurate measurement of the magnitude or shift of a single resonance. The magnitude and frequency shift of a single resonance can also be affected by the position of the tag relative to the reader antenna (illustrated in Fig 21), making it challenging to isolate the effect of the sensing parameter when looking at a singular resonance [24].

It should be noted that as shown in Fig. 12c, increasing the loss factor (i.e., loss tangent) removes some of the notches from the overall resonance response, particularly at higher frequencies (i.e., consistent with increase in R in an RLC circuit resulting in a decrease in its Q-factor).Therefore, any tag design must be made with this issue in mind (i.e., loss associated with the material of interest in which a tag may be embedded). Additionally, this indicates a limitation as to how lossy materials can be used with this tag when attempting to perform materials characterization.

Other ways to perform materials characterization with this response are to consider the resonance frequency of the stop bit or to look at how the distance between two notches changes. These two methods can provide information about permittivity, but cannot be used to determine loss factor unless the measurement of the magnitude of the response can be trusted [33–35]. It should be noted that all of these chipless RFID materials characterization approaches are less mature than other microwave materials characterization approaches, such as the open-ended waveguide method and the ring-resonator method [36, 37]. Therefore, less accuracy can be expected from these chipless RFID methods. However, these methods provide a quick, inexpensive, wireless and a passive way to characterize dielectric materials and examine how the dielectric properties change over time (i.e., temporal changes), and therefore deserve further exploration.

In order to optimize the tag in Fig. 11 for ID applications, the detuning strategy discussed previously was used. This allows for the response to be robust to the removal of spirals, which is a desirable feature for ID-based tags since it means that the full possible number of unique codes can be generated for the tag. Figs. 13a–d show four different configurations of the tag to demonstrate the tag’s suitability for ID and Figs. 14a–d show the frequency response in free-space (Fig. 14a) and for three different cases when removing spirals (Figs. 14b–d) for the tag configurations shown in Fig. 13. This removal of spirals is done for the purpose of creating different RCS vs. frequency responses and therefore different codes and IDs.

In these cases, the removed spiral numbering refers to the notch frequency order (i.e., the length of the spiral, with the longest spiral being spiral 1) rather than the location around the spiral like was done in Fig. 7. By examining the cases in Figs. 14a–d it can be seen that the response is relatively robust to the removal of a spiral. The resonance associated with the removed spiral is removed from the response, but the surrounding resonances do not shift significantly or disappear. This also speaks to the great deal of control over the tag response that can be achieved with this detuning strategy. This control is extremely advantageous in that it allows for easy modification of tag designs to fit new applications.

V. Tag Geometry and Tag Response Association

Based on the preceding discussions, it is clearly evident that when multiple types of element classes are used in a tag design, the interactions between them are complex and cannot be described analytically. Even through simulations, it can be difficult to discern which response characteristics are associated with which tag element. This in turn makes it difficult to determine which tag element needs to be modified to create a desired tag response.

However, the study of surface current density associated with the irradiated tags can be useful in this understanding. Surface current density has been used to illustrate how tags operate, such as in Fig. 5, but it has not been explicitly used to associate tag geometry with response characteristics [11, 38, 39]. The surface current density can then be viewed at frequencies where there is a resonance in the response and in doing so the tag element associated with that resonance can be isolated. Fig 15, features the lower frequency version of the 8 spiral tag whose model was shown in Fig. 13a, with its free-space frequency response shown in Fig. 14a. Figs. 15a–f show the surface current density associated with the spiral elements of the tag at six different frequencies. From these plots, one can associate a certain tag response characteristic with a specific tag element. For example, Fig. 15a shows a high surface current density associated with the top spiral tag element. This simulation result is for 10.2 GHz where there happens to also be a deep notch in the RCS vs. frequency response that is shown in Fig. 14a. The results also show the sensitivity of other tag elements to different irradiating frequencies, indicating such analysis to be a useful tool for designing tags that incorporate multiple types of resonators.

VI. Tag Metrics

A. Current Tag Metrics

Currently, there exist a few popular tag metrics, namely: bit density, coding capacity, and data capacity that are used to evaluate various tag attributes. Bit density is the number of bits per centimeter squared of tag area, while coding capacity has multiple reported definitions. One of these definitions refers to coding capacity as it relates to the number of total combinations of bits, which mathematically is expressed as [40]:

$$2^{C} = \text{Total Combination} \tag{1}$$

This equation can be rearranged to get:

$$C = \log(T)/\log(2) \tag{2}$$

T in (2) refers to the total number of combinations for codes, and is determined by multiplying the number of possible positions for each resonance (i.e., multiplying the number of possible defined positions for the first notch in the response by the number of possible positions for the second notch in the response and so on). By doing so, this definition takes into account the multiple positions a notch can take in the frequency response of the tag, but is dependent on how the code generator determines what constitutes a different position for a resonance.

Another definition simply provides the total number of possible combinations [41]. This definition can be mathematically expressed as:

$$2^{n} = \text{Coding Capacity} \tag{3}$$

In this equation, n refers to the number of bits in the code.

A third definition used for a case where a frequency shift encoding (FSE) mechanism is used incorporates the number of resonators, the bandwidth used for the tag response, and the average bandwidth of the notches in the response to determine the coding capacity, as following [42]:

$$(f/\Delta f)^{n} = 2^{C} \tag{4}$$

In (4), f represents the bandwidth of the tag response, Δf represents the frequency difference between two coding locations in the response, n represents the number of resonances, and C represents the coding capacity. This definition is dependent on using the FSE mechanism described in [42] and cannot easily be extended to scenarios where other coding methods are used.

A fourth definition divides the tag response bandwidth by the number of positions a single resonance in the spectral response of the tag could take. In this sense, coding capacity is the maximum possible number of resonances that could be achieved using a single element class within a certain bandwidth. The context in which this definition was proposed, is a scenario where an FSE like coding mechanism is again used like was used in the third presented definition of coding capacity [43].

Data capacity is a third metric that is used less commonly than bit density and coding capacity. In the cases when it has been used, it has been referred to as the number of bits in the code [3]. This definition does not take into account the size of the tag as does bit density. It is, however, still highly dependent on the code generation method used, similar to the previously-presented bit density and second definition of coding capacity. A fourth metric that is used infrequently is spectral density. Spectral density or spectral capacity is considered to be the number of bits in the code per bandwidth used for encoding [29]. All four of these metrics were designed for measuring the suitability of a tag for ID applications. They do not indicate the suitability of a tag for sensing applications or how practically usable the tag is in terms of reader system requirements.

Based on the definition of bit density and the second definition of coding capacity, it is obvious that these metrics depend on the length of the code associated with a tag and therefore they are coding method-dependent metrics. Additionally, utilizing bandwidth before or after the last notch in the response can yield longer codes making these metrics also dependent on how the coding method is implemented. These facts are often overlooked when comparing tags and lead to unfair (i.e., not one-to-one) comparisons. Thus, the bit density and coding capacity from definition 2 for the 8 spiral tag in Fig. 3c are reported in Table I for the following popular coding methods as well as a coding method developed for embedded materials characterization:

1. Coding method 1 – notches are 1s, removing a notch shortens the code [44].
2. Coding method 2 – notches are 1s, removing a notch, adds a 0 to the code [12].
3. Coding method 3 – notches are 1s, elsewhere are 0s [45].
4. Coding method 4 – Frequency Shift Encoding: bit sequences are assigned to each notch depending on its position state. Position states refer to the user-defined set of resonant frequencies a notch can have in a response. The assigned bit sequences are concatenated together [42].
5. Coding method 5 – the response bandwidth is divided into windows based on the narrowest notch in the response and then 1s and 0s are assigned based on the portion of the response above and below a threshold in each window. This produces a code that is very sensitive to shifts in response, a feature that is desirable when trying to determine dielectric properties (i.e., for materials characterization) [30].
6. Coding Method 6 – extends FSE to both amplitude and phase data to create a hybrid coding method [46].

As previously mentioned, these tag metrics are very dependent on the coding method used and are also dependent on how a tag designer employs the coding method. This point is illustrated by the extreme variation in the metrics in Table I, where version 1 is the tag in Fig 9b and version 2 is the tag in Fig 11a. Overall, these variations in metric usage make it difficult to compare tags based on their reported metrics.

Therefore, the context of the coding method is needed if to make proper comparison among the tags. Table II shows how the achieved bit density compares to that of some other tags. As can be seen, the achieved bit density with the version 1 8-spiral tag is very high and to the best of the author's knowledge, it is the highest yet to be reported.

B. Proposed Tag Metrics

The current tag metrics were designed to be used for ID application tags and are therefore limited when it comes to describing the performance of sensing tags. These current metrics also fail to describe the measurability of the tag, which is important for using tags outside of a controlled laboratory environment. Due to these limitations, three new tag metrics are proposed.

The first proposed metric is a modification of the bit density metric, namely; notch density. Notch density is defined as the number of notches in the response per tag area and response bandwidth used. For the case of the proposed tag, the notch density would be 10/0.36 cm^2/19 GHz. This concisely conveys the coding potential, the size of the tag, and the bandwidth needed to read the tag and this information together provides insight into the practicality of the tag. Additionally, this metric removes the coding method dependency and much of the bias by code assigner (i.e., the dependency of the code on how the assigner applies the chosen coding method).

Average Q-factor is another proposed metric that plays into the measurability of a tag. If the notches are narrow, a certain number of frequency points are need to be used by the reader system to ensure that the response features are properly captured. If too few frequency points are used, a notch can be missed leading to bit errors and generation of incorrect codes.

A third possible tag measurement is the maximum RCS value in the tag response bandwidth. The higher the RCS of the tag is, the easier it is to measure the tag and distinguish its response from that of the background response. Additionally, the reader system being used will have a certain level of sensitivity so this metric could tell the user if a tag could be used with the reader system they have available to them.

Lastly, measurand sensitivity could be used as metric more frequently with sensing-based chipless RFID tags. Sensitivity can be defined as the extent to which a sensor response changes as a function of the measurand. This could be used to compare the performance of sensing tags that are designed to sense the same measurand and could thus be used to determine which tag is best suited for the application at hand.

VII. Measurement

The lower frequency version of the tag, shown in Fig. 11a with its free-space response shown in Fig. 11b, was manufactured through a commercial PCB fabrication house. Additionally, a single spiral configuration, like the one that was previously utilized in section III, was manufactured. Both tags were manufactured on Rogers 4350B dielectric material, which has a permittivity of 3.48 and a loss tangent of 0.0037, for a cost of ~$90 per tag. The use of slightly higher permittivity substrate, than that used in the original design, causes the response of the tag to compress slightly in frequency and for this reason, the simulated S_{11} responses for these tags with a waveguide as the reader antenna are shown in Fig. 16b. The simulation setup is shown in Fig. 16a. It should also be noted that the cost per tag could be reduced substantially by utilizing bulk fabrication or by employing inkjet-printing as a means of manufacturing. To place this in context, with inkjet-printing the cost of materials per tag would be approximately $0.008 based on using Mitsubishi paper as the substrate and NBSIJ-FD02 silver nanoparticle ink.

As previously mentioned, RCS is typically used for chipless RFID simulations due to its distance independence. However, RCS is challenging to measure in practice and many of the methods for doing so would not be practical outside of a laboratory setting. For example, the method described in [9] requires measurements to be made of the S_{11} of a reference target, the S_{11} of the environment without the tag, and the S_{11} of the tag. A formula is then used to calculate the RCS from these measured parameters (i.e., not a direct RCS measurement). If this method were to be employed for an embedded materials characterization application, though, the reference target would need to be able to be embedded at the same location as the tag, then removed and replaced with the tag. For expected applications, such as embedding in the concrete of a civil structure, this is not feasible. For ID applications, the main target application is supply-chain management. To utilize this RCS measurement method in this application would require that the tag adhered to a product be replaced by a reference target and for additional measurements to be made for each product, which would

be time consuming, especially in comparison to the measurement techniques used with passive RFID tags [52]. Thus, RC S measurements are limited in terms of speed, complexity, and feasibly in some applications. Consequently, S_{11} is used for these simulations and in subsequent measurements due to its relative simplicity compared to making accurate RCS measurements. The manufactured tags are shown in Fig. 17. Five copies of each tag were made and used during measurement to verify the consistency of the manufacturing process.

Measurements were conducted for both of these tag designs using an X-band (8.2–12.4 GHz) waveguide with a modified flange described in [53], which significantly reduced unwanted reflections from flange edges, and an Anritsu MS4644A VectorStar vector network analyzer (VNA). The tag was adhered to a piece of absorbing foam using double stick tape and placed in front of the waveguide at a distance of 0.5 cm. During the measurements, the waveguide was operated outside of its typical range from 7.5–12.4 GHz (cutoff frequency is 6.56 GHz) to capture the first notch and 3001 frequency points were measured. The measurement setup is shown in Fig. 18. In processing the data, the response of the foam was (coherently) subtracted from the response of the tag. All five copies of each tag design were measured producing similar results. Thus, the measurement results for only one of each design are presented for brevity. The processed measurement results in comparison to their simulated results are shown in Fig. 19. Ovals are used to indicate which simulated resonance is believed to correspond to which measured resonance.

From Fig. 19a, good agreement between simulation and measurement results are obtained for the single spiral tag. In Fig. 19b, one notch is missing in the response, however, the remaining notches are in similar locations to those in the simulation. In the measurement case, however, the notches are not very deep. This can potentially make it difficult to practically associate a binary code with the response due to the lack of discernibility of some of the notches. The differences between the simulation and measurement results and the low level of some of the notches for the 8-spiral tag was consistent for all five copies of the 8-spiral tag that were measured. We believe the discrepancy between the simulated and measured results is primarily caused by manufacturing tolerances (i.e., spiral resonators are slightly longer or shorter than they should be causing a shift in resonance frequency or destructive interference leading to a missing notch), misalignment between the waveguide and tag, or a combination of both. To this end, additional simulations were conducted in which the overall lengths of three of the spirals (in positions 1, 3 and 5 in Fig. 7) were decreased by 0.076 mm (i.e., the minimum feature size capability of the PCB manufacturer). These results are shown in Fig. 20. As can be seen, in Fig. 20, the three notches associated with the three modified spirals have shifted up in frequency. This confirms that manufacturing inaccuracies could be a source of the disagreement between the simulation and measurement. Subsequently, simulations were conducted in which the tag was translated and rotated with respect to the waveguide. Fig. 21 shows simulation results for two cases (i.e., the case for which the tag is translated in the +x direction and the case for which the tag is rotated about the x-axis) to illustrate the effect that misalignment can potentially have.

Additional misalignment simulation results are provided in [24]. From these simulations it was found that X and Y translation tend to change the magnitude of the response

while rotation about the X, Y, and Z axes tends to cause shifts in notches and changes in response shape. This indicates that misalignment could indeed also be playing a role in the disagreement between the simulation and measurement results. Furthermore, [24] provides additional measurement results for ID and embedded materials characterization applications.

VIII. Conclusion

In this paper, a novel application-adaptable tag design methodology was presented along with new analysis of a tag that combines multiple types of resonators. The efficacy of this methodology, using the presented spiral tag was illustrated for both embedded and ID applications. Furthermore, a method for associating tag response characteristics with individual tag elements was presented, and new tag metrics were defined and used to describe the usefulness of tag design. Extensive numerical simulations were conducted to study the various features of such tag designs and the results were compared with experiments using similarly manufactured tags.

It was shown that by combining multiple types of resonators, and having an understanding of how tag elements interact with each other and how the environment affects the overall tag performance, tags with greater versatility, functionality, and application-adaptability can be designed. Additionally, measurement challenges associated with chipless RFID were explored. It was seen that small misalignments or manufacturing inaccuracies can cause large differences in tag response and the limitations of RCS measurement when it comes to embedded materials characterization and ID applications were discussed.

Future work will include delving into exploiting the polarization dependency of this tag to perform rotation sensing, developing a greater understanding of the interactions between resonating elements, performing more measurements, and using this tag as an embedded materials characterization sensor. Additionally, methods to increase the speed and accuracy of RCS measurement in practical application settings (i.e., outside of the laboratory) will be explored so that distance dependence in measurement can be overcome. Overcoming other measurement challenges, such as read range and tag localization, will also be explored by examining traditional RFID solutions. In doing so, the chipless RFID field will be explored in the context of metrological and sensing concepts like uncertainty, stability, sensitivity, and response time. Furthermore, increasing the bit density by creating a 12-spiral tag is worthy of pursuit in the future for evaluating potential usefulness of having a greater bit density for sensing applications. Other potential areas of investigation include examining humidity and temperature sensitivity and modifying the tag to sense multiple environmental parameters.

Acknowledgments

This work was supported by a NASA Space Technology Research Fellowship.

Biographies

K. Brinker received her B.S. degrees in electrical engineering and computer engineering in 2017, and her M.S. degree in electrical engineering in 2019 from Missouri University of Science and Technology (Missouri S&T). Currently, she is working on her Ph.D. in electrical engineering with the support of a NASA Space Technology Research Fellowship. She has served as the Undergraduate Student Representative and Graduate Student Representative to the AdCom of the IEEE Instrumentation and Measurement Society and as a Student Governor to the Board of Governors for IEEE-HKN. She is also the recipient of the 2017 IEEE-HKN Alton B. Zerby and Carl T. Koerner Outstanding Student Award, the 2017 IEEE-USA recipient of the DiscoverE New Faces of Engineering Award, and the 2018 IEEE St. Louis Section Outstanding Graduate Student Award.

M. Vaccaro is a senior in an Electrical Engineering program at Missouri University of Science and Technology. He currently works in the Applied Microwave Nondestructive Testing Laboratory on campus as a research assistant, and previously worked in applied electromagnetics at Los Alamos National Laboratory during a summer internship.

R. Zoughi (S’85-M’86-SM’93-F’06) received his B.S.E.E, M.S.E.E, and Ph.D. degrees in electrical engineering (radar remote sensing, radar systems, and microwaves) from the University of Kansas where from 1981 until 1987 he was at the Radar Systems and Remote Sensing Laboratory (RSL). Currently he is the *Schlumberger Endowed Professor* of Electrical and Computer Engineering at Missouri University of Science and Technology (Missouri S&T). Prior to joining Missouri S&T in January 2001 and since 1987 he was with the Electrical and Computer Engineering Department at Colorado State University (CSU), where he was a professor and established the Applied Microwave Nondestructive Testing Laboratory (*amntl*) (http://amntl.mst.edu/). Dr. Zoughi held the position of *Business Challenge Endowed Professor* of Electrical and Computer Engineering from 1995 to 1997 while at CSU.

While at CSU he received nine teaching awards, including the *State Board of Agriculture, Excellence in Undergraduate Teaching Award* and the *Abell Faculty Teaching Award*. Since at Missouri S&T he has received seventeen *Outstanding Teaching Awards & Commendations*. He is the recipient of the 2007 IEEE Instrumentation and Measurement Society *Distinguished Service Award*, the 2009 American Society for Nondestructive Testing (ASNT) *Research Award for Sustained Excellence* and the 2011 *IEEE Joseph*

F. Keithley Award in Instrumentation and Measurement. In 2013 he and his co-authors received the *H. A. Wheeler Applications Prize Paper Award* from the IEEE Antennas and Propagation Society (APS).

He is the author of a textbook entitled "*Microwave Nondestructive Testing and Evaluation Principles*" KLUWER Academic Publishers, 2000, and the co-author of a chapter on Microwave Techniques in the book entitled "*Nondestructive Evaluation: Theory, Techniques, and Applications*" Marcel and Dekker, Inc., 2002. He is the co-author of over 634 journal papers, conference proceedings and presentations and technical reports.

He served as the *Editor-in-Chief* of the IEEE Transactions on Instrumentation and Measurement (2007–2011), two terms as an *at-large AdCom member* of the IEEE Instrumentation and Measurement (I&M) Society, *I&M Society President* (2014–2015) and serves as an *I&M Society Distinguished Lecturer*. He served as the *General Co-Chair* of the 2013 IEEE Instrumentation and Measurement Technology Conference (I^2MTC). He has been elected as an *at-large member of IEEE Publications Services & Products Board (PSPB)* for two terms (2016–2018 & 2019–2021), and served on the *IEEE TAB/PSPB* (2015 & 2017–2019).

He has eighteen issued US patents to his credit (with several issued abroad) in the field of microwave nondestructive testing and evaluation. He has delivered numerous *Invited* and *Keynote* presentations on the subject of microwave and millimeter wave nondestructive testing and imaging. He is also a *Fellow* of the American Society for Nondestructive Testing (ASNT).

REFERENCES

[1]. Mukherjee S, "Chipless Radio Frequency Identification (RFID) Device," in 2007 1st Annual RFID Eurasia, 5–6 Sept. 2007 2007, pp. 1–4, doi: 10.1109/RFIDEURASIA.2007.4368096.

[2]. Preradovic S and Karmakar N, Multiresonator-Based Chipless RFID Barcode of the Future. Springer 2012.

[3]. Islam MA and Karmakar NC, "Real-World Implementation Challenges of a Novel Dual-Polarized Compact Printable Chipless RFID Tag," IEEE Transactions on Microwave Theory and Techniques, vol. 63, no. 12, pp. 4581–4591, 2015, doi: 10.1109/TMTT.2015.2495285.

[4]. Costa F et al. , "Design of wireless sensors by using chipless RFID technology," in 2017 Progress In Electromagnetics Research Symposium - Spring (PIERS), 22–25 May 2017 2017, pp. 3309–3313, doi: 10.1109/PIERS.2017.8262327.

[5]. Vena A, Tedjini M, Björninen T, Sydänheimo L, Ukkonen L, and Tentzeris MM, "A novel inkjet-printed wireless chipless strain and crack sensor on flexible laminates," in 2014 IEEE Antennas and Propagation Society International Symposium (APSURSI), 6–11 July 2014 2014, pp. 1294–1295, doi: 10.1109/APS.2014.6904974.

[6]. Borgese M, Dicandia FA, Costa F, Genovesi S, and Manara G, "An Inkjet Printed Chipless RFID Sensor for Wireless Humidity Monitoring," IEEE Sensors Journal, vol. 17, no. 15, pp. 4699–4707, 2017, doi: 10.1109/JSEN.2017.2712190.

[7]. Khaliel M, El-Awamry A, Megahed AF, and Kaiser T, "A Novel Design Approach for Co/Cross-Polarizing Chipless RFID Tags of High Coding Capacity," IEEE Journal of Radio Frequency Identification, vol. 1, no. 2, pp. 135–143, 2017, doi: 10.1109/JRFID.2017.2765560.

[8]. Vena A, Perret E, and Tedjini S, "A Fully Printable Chipless RFID Tag With Detuning Correction Technique," IEEE Microwave and Wireless Components Letters, vol. 22, no. 4, pp. 209–211, 2012, doi: 10.1109/LMWC.2012.2188785.

[9]. Hotte D, Siragusa R, Duroc Y, and Tedjini S, “Radar cross-section measurement in millimetre-wave for passive millimetre-wave identification tags,” IET Microwaves, Antennas & Propagation, vol. 9, no. 15, pp. 1733–1739, 2015, doi: 10.1049/ietmap.2015.0281.

[10]. Wiesbeck W and Kahny D, “Single reference, three target calibration and error correction for monostatic, polarimetric free space measurements,” Proceedings of the IEEE, vol. 79, no. 10, pp. 1551–1558, 1991, doi: 10.1109/5.104229.

[11]. Vena A, Perret E, and Tedjini S, “High-Capacity Chipless RFID Tag Insensitive to the Polarization,” IEEE Transactions on Antennas and Propagation, vol. 60, no. 10, pp. 4509–4515, 2012, doi: 10.1109/TAP.2012.2207347.

[12]. Islam MA, Yap Y, Karmakar N, and Azad AKM, “Orientation independent compact chipless RFID tag,” in 2012 IEEE International Conference on RFID-Technologies and Applications (RFID-TA), 5–7 Nov. 2012 2012, pp. 137–141, doi: 10.1109/RFID-TA.2012.6404499.

[13]. Kalansuriya P, Karmakar NC, and Viterbo E, “On the Detection of Frequency-Spectra-Based Chipless RFID Using UWB Impulsed Interrogation,” IEEE Transactions on Microwave Theory and Techniques, vol. 60, no. 12, pp. 4187–4197, 2012, doi: 10.1109/TMTT.2012.2222920.

[14]. Koswatta RV and Karmakar NC, “A Novel Reader Architecture Based on UWB Chirp Signal Interrogation for Multiresonator-Based Chipless RFID Tag Reading,” IEEE Transactions on Microwave Theory and Techniques, vol. 60, no. 9, pp. 2925–2933, 2012, doi: 10.1109/TMTT.2012.2203929.

[15]. Koswatta R and Karmakar NC, “Investigation into antenna performance on read range improvement of chipless RFID tag reader,” in 2010 Asia-Pacific Microwave Conference, 7–10 Dec. 2010 2010, pp. 1300–1303.

[16]. Fawky A, El-Awamry A, Khaliel M, and Kaiser T, “Novel notch detection techniques for Frequency Coded chipless RFID,” in 2017 IEEE 14th International Conference on Networking, Sensing and Control (ICNSC), 16–18 May 2017 2017, pp. 345–350, doi: 10.1109/ICNSC.2017.8000116.

[17]. Rezaiesarlak R and Manteghi M, “Short-Time Matrix Pencil Method for Chipless RFID Detection Applications,” IEEE Transactions on Antennas and Propagation, vol. 61, no. 5, pp. 2801–2806, 2013, doi: 10.1109/TAP.2013.2238497.

[18]. Costa F, Genovesi S, and Monorchio A, “Reading chipless RFID located on metallic platforms by using cross-polar scattering,” in 2014 XXXIth URSI General Assembly and Scientific Symposium (URSI GASS), 16–23 Aug. 2014 2014, pp. 1–4, doi: 10.1109/URSIGASS.2014.6929188.

[19]. Palazzi V et al. , “Demonstration of a high dynamic range chipless RFID sensor in paper substrate based on the harmonic radar concept,” in 2015 IEEE MTT-S International Microwave Symposium, 17–22 May 2015 2015, pp. 1–4, doi: 10.1109/MWSYM.2015.7166933.

[20]. Scherhäufl M, Pichler M, and Stelzer A, “UHF RFID Localization Based on Evaluation of Backscattered Tag Signals,” IEEE Transactions on Instrumentation and Measurement, vol. 64, no. 11, pp. 2889–2899, 2015, doi: 10.1109/TIM.2015.2440554.

[21]. Whitney AM, Parker JM, Kratzer ZCN, Fessler JT, and Whitney JG, “Reducing RF Distance Error by Characterizing Multipath,” IEEE Transactions on Instrumentation and Measurement, pp. 1–10, 2018, doi: 10.1109/TIM.2018.2875899.

[22]. Li B, He Y, Zuo L, and Long Y, “Metric of the Application Environment Impact to the Passive UHF RFID System,” IEEE Transactions on Instrumentation and Measurement, vol. 63, no. 10, pp. 2387–2395, 2014, doi: 10.1109/TIM.2013.2287119.

[23]. Brinker K and Zoughi R, “Application-Adaptable Chipless RFID Tag,” in Proceedings of the IEEE International Symposium on Antennas and Propagation (AP-S), Boston, MA, July 8–13, 2018 2018, pp. 1493–1494.

[24]. Brinker K, “Passively-Coded Embedded Microwave Sensors for Materials Characterization and Structural Health Monitoring (SHM),” Master of Science Electrical Engineering, Electrical and Computer Engineering, Missouri University of Science and Technology, 2019.

[25]. Martinez M and Weide D. v. d., “Compact slot-based chipless RFID tag,” in 2014 IEEE RFID Technology and Applications Conference (RFID-TA), 8–9 Sept. 2014 2014, pp. 233–236, doi: 10.1109/RFID-TA.2014.6934234.

[26]. Gu Q, Wan GC, Gao C, and Tong MS, “Frequency-coded chipless RFID tag based on spiral resonators,” in 2016 Progress in Electromagnetic Research Symposium (PIERS), 8–11 Aug. 2016 2016, pp. 844–846, doi: 10.1109/PIERS.2016.7734499.

[27]. Araújo L. d. S. and Oliveira A. J. B. d., “The square spiral resonator: Investigating its electromagnetic performance for filter design,” in 2015 SBMO/IEEE MTT-S International Microwave and Optoelectronics Conference (IMOC), 3–6 Nov. 2015 2015, pp. 1–6, doi: 10.1109/IMOC.2015.7369227.

[28]. Brinker K and Zoughi R, “Measurement of Inkjet-Printing Parameters for Accurate Chipless RFID Tag EM Simulation,” in IEEE International Instrumentation and Measurement Technologies Conference, Auckland, New Zealand, 2019.

[29]. Issa K et al. , “A High-Density L-Shaped Backscattering Chipless Tag for RFID Bistatic Systems,” International Journal of Antennas and Propagation, vol. 2018, 2018.

[30]. Brinker K and Zoughi R, “Embedded chipless RFID measurement methodology for microwave materials characterization,” in 2018 IEEE International Instrumentation and Measurement Technology Conference (I2MTC), 14–17 May 2018 2018, pp. 1–6, doi: 10.1109/I2MTC.2018.8409670.

[31]. Santos-Souza GT, Alves A. A. d. C., Bravo-Roger LL, and Hernandez-Figueroa HE, “Numerical determination of frequency guard band resonances for Chipless RFID Tags,” in 2014 IEEE Brasil RFID, 25–25 Sept. 2014 2014, pp. 10–12, doi: 10.1109/BrasilRFID.2014.7128952.

[32]. Genovesi S, Costa F, Borgese M, Dicandia FA, Monorchio A, and Manara G, “Chipless RFID sensor for rotation monitoring,” in 2017 IEEE International Conference on RFID Technology & Application (RFID-TA), 20–22 Sept. 2017 2017, pp. 233–236, doi: 10.1109/RFID-TA.2017.8098885.

[33]. Capdevila S, Jofre L, Romeu J, and Bolomey JC, “RFID array sensing,” in Proceedings of the Fourth European Conference on Antennas and Propagation, 12–16 April 2010 2010, pp. 1–5.

[34]. Suwalak R, Lertsakwimarn K, Phongcharoenpanich C, and Torrungrueng D, “Dual-band chipless RFID sensor for a material quality monitoring application,” in 2016 International Symposium on Antennas and Propagation (ISAP), 24–28 Oct. 2016 2016, pp. 1004–1005.

[35]. Cataldo A, Monti G, Benedetto ED, Cannazza G, and Tarricone L, “A Noninvasive Resonance-Based Method for Moisture Content Evaluation Through Microstrip Antennas,” IEEE Transactions on Instrumentation and Measurement, vol. 58, no. 5, pp. 1420–1426, 2009, doi: 10.1109/TIM.2009.2014513.

[36]. Ghasr MT, Simms D, and Zoughi R, “Multimodal Solution for a Waveguide Radiating Into Multilayered Structures—Dielectric Property and Thickness Evaluation,” IEEE Transactions on Instrumentation and Measurement, vol. 58, no. 5, pp. 1505–1513, 2009, doi: 10.1109/TIM.2008.2009133.

[37]. Bernard PA and Gautray JM, “Measurement of dielectric constant using a microstrip ring resonator,” IEEE Transactions on Microwave Theory and Techniques, vol. 39, no. 3, pp. 592–595, 1991, doi: 10.1109/22.75310.

[38]. Huang H and Su L, “A Compact Dual-Polarized Chipless RFID Tag by Using Nested Concentric Square Loops,” IEEE Antennas and Wireless Propagation Letters, vol. 16, pp. 1036–1039, 2017, doi: 10.1109/LAWP.2016.2618928.

[39]. Javed N, Habib A, Amin Y, and Tenhunen H, “Miniaturized flexible chipless RFID tag for IoT market,” in 2017 International Conference on Communication, Computing and Digital Systems (C-CODE), 8–9 March 2017 2017, pp. 71–74, doi: 10.1109/C-CODE.2017.7918904.

[40]. Khan MM, Tahir FA, Farooqui MF, Shamim A, and Cheema HM, “3.56-bits/cm Compact Inkjet Printed and Application Specific Chipless RFID Tag,” IEEE Antennas and Wireless Propagation Letters, vol. 15, pp. 1109–1112, 2016, doi: 10.1109/LAWP.2015.2494864.

[41]. Mumtaz M, Amber SF, Ejaz A, Habib A, Jafri SI, and Amin Y, “Design and analysis of C shaped chipless RFID tag,” in 2017 International Symposium on Wireless Systems and Networks (ISWSN), 19–22 Nov. 2017 2017, pp. 1–5, doi: 10.1109/ISWSN.2017.8250009.

[42]. Bao H and Liu X, “A depolarizing chipless RFID tag with quasi-loop resonators,” in 2017 IEEE International Symposium on Antennas and Propagation & USNC/URSI

National Radio Science Meeting, 9–14 July 2017 2017, pp. 2513–2514, doi: 10.1109/APUSNCURSINRSM.2017.8073299.

[43]. Khan MM, Tahir FA, and Cheema HM, "High capacity polarization sensitive chipless RFID tag," in 2015 IEEE International Symposium on Antennas and Propagation & USNC/URSI National Radio Science Meeting, 19–24 July 2015 2015, pp. 1770–1771, doi: 10.1109/APS.2015.7305274.

[44]. Habib A, Afzal MA, Sadia H, Amin Y, and Tenhunen H, "Chipless RFID tag for IoT applications," in 2016 IEEE 59th International Midwest Symposium on Circuits and Systems (MWSCAS), 16–19 Oct. 2016 2016, pp. 1–4, doi: 10.1109/MWSCAS.2016.7870033.

[45]. Preradovic S, Balbin I, Karmakar NC, and Swiegers G, "A Novel Chipless RFID System Based on Planar Multiresonators for Barcode Replacement," in 2008 IEEE International Conference on RFID, 16–17 April 2008 2008, pp. 289–296, doi: 10.1109/RFID.2008.4519383.

[46]. Vena A, Perret E, and Tedjini S, "Chipless RFID Tag Using Hybrid Coding Technique," IEEE Transactions on Microwave Theory and Techniques, vol. 59, no. 12, pp. 3356–3364, 2011, doi: 10.1109/TMTT.2011.2171001.

[47]. Costa F, Genovesi S, and Monorchio A, "A Chipless RFID Based on Multiresonant High-Impedance Surfaces," IEEE Transactions on Microwave Theory and Techniques, vol. 61, no. 1, pp. 146–153, 2013, doi: 10.1109/TMTT.2012.2227777.

[48]. Necibi O, Naoui S, and Gharsallah A, "Design of a chipless RFID TAG based on the frequency shift technique for K band," in 2016 2nd International Conference on Advanced Technologies for Signal and Image Processing (ATSIP), 21–23 March 2016 2016, pp. 816–819, doi: 10.1109/ATSIP.2016.7523194.

[49]. Anam H, Habib A, Jafri SI, Amin Y, and Tenhunen H, "Directly Printable Frequency Signatured Chipless RFID Tag for IoT Applications," RADIOENGINEERING, vol. 26, no. 1, 2017.

[50]. Svanda M, Havlicek J, Machac J, and Polivka M, "Polarisation independent chipless RFID tag based on circular arrangement of dual-spiral capacitively-loaded dipoles with robust RCS response," IET Microwaves, Antennas & Propagation, vol. 12, no. 14, pp. 2167–2171, 2018, doi: 10.1049/iet-map.2018.5434.

[51]. Zeb S, Satti JA, Habib A, Amin Y, and Tenhunen H, "Dual-polarized data dense chipless RFID tag towards IoT applications," in 2017 International Symposium on Wireless Systems and Networks (ISWSN), 19–22 Nov. 2017 2017, pp. 1–5, doi: 10.1109/ISWSN.2017.8250038.

[52]. Ramakrishnan KM and Deavours DD, "Performance Benchmarks for Passive UHF RFID Tags," in 13th GI/ITG Conference - Measuring, Modelling and Evaluation of Computer and Communication Systems, 27–29 March 2006 2006, pp. 1–18.

[53]. Kempin M, Ghasr MT, Case JT, and Zoughi R, "Modified Waveguide Flange for Evaluation of Stratified Composites," IEEE Transactions on Instrumentation and Measurement, vol. 63, no. 6, pp. 1524–1534, 2014, doi: 10.1109/TIM.2013.2291952.

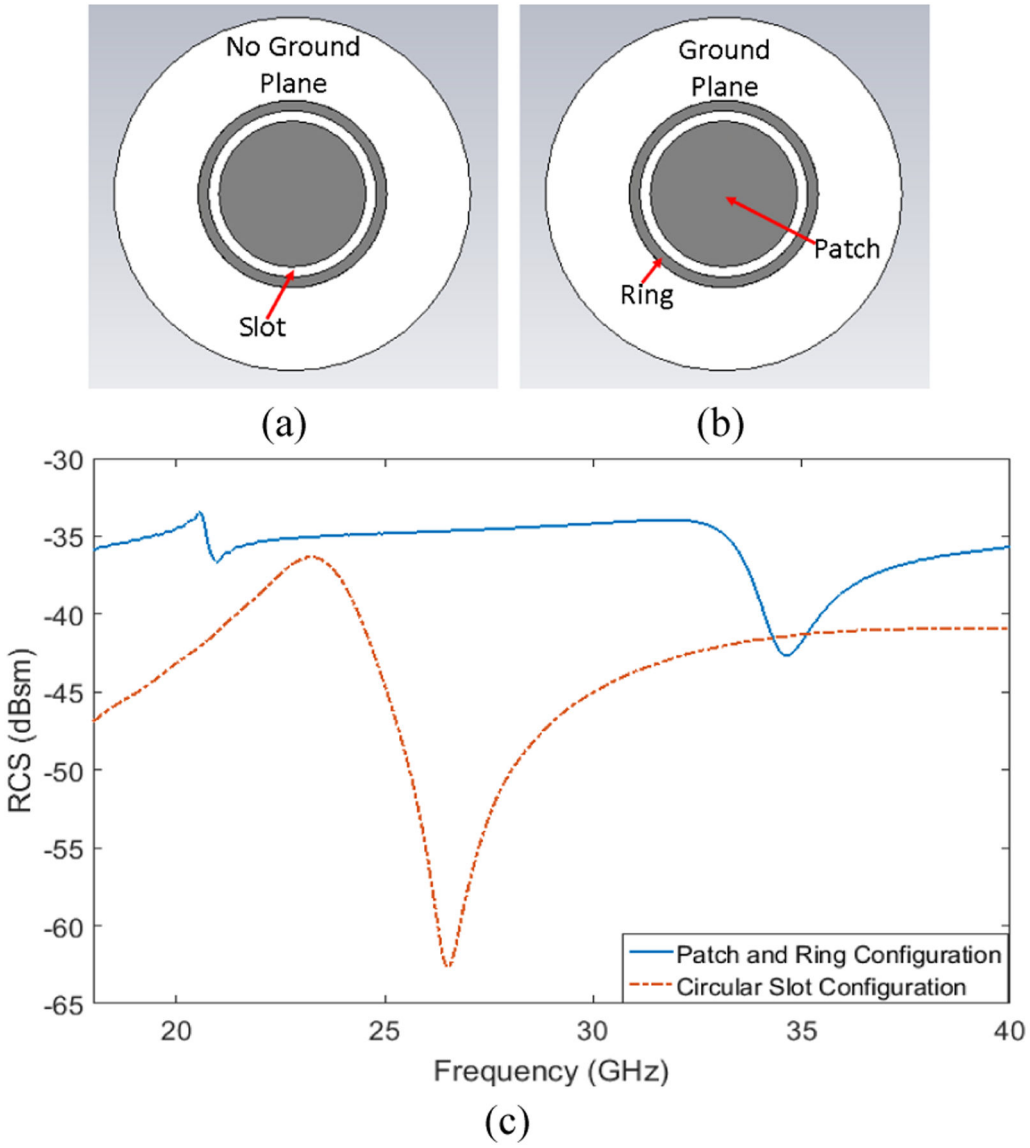

Fig. 1:

Effect of ground plane on slot and ring resonators: a) model of a circular slot resonator tag with no ground plane, b) model of a ring resonator and patch antenna tag with a ground plane, and c) comparison of responses for tag with and without ground plane.

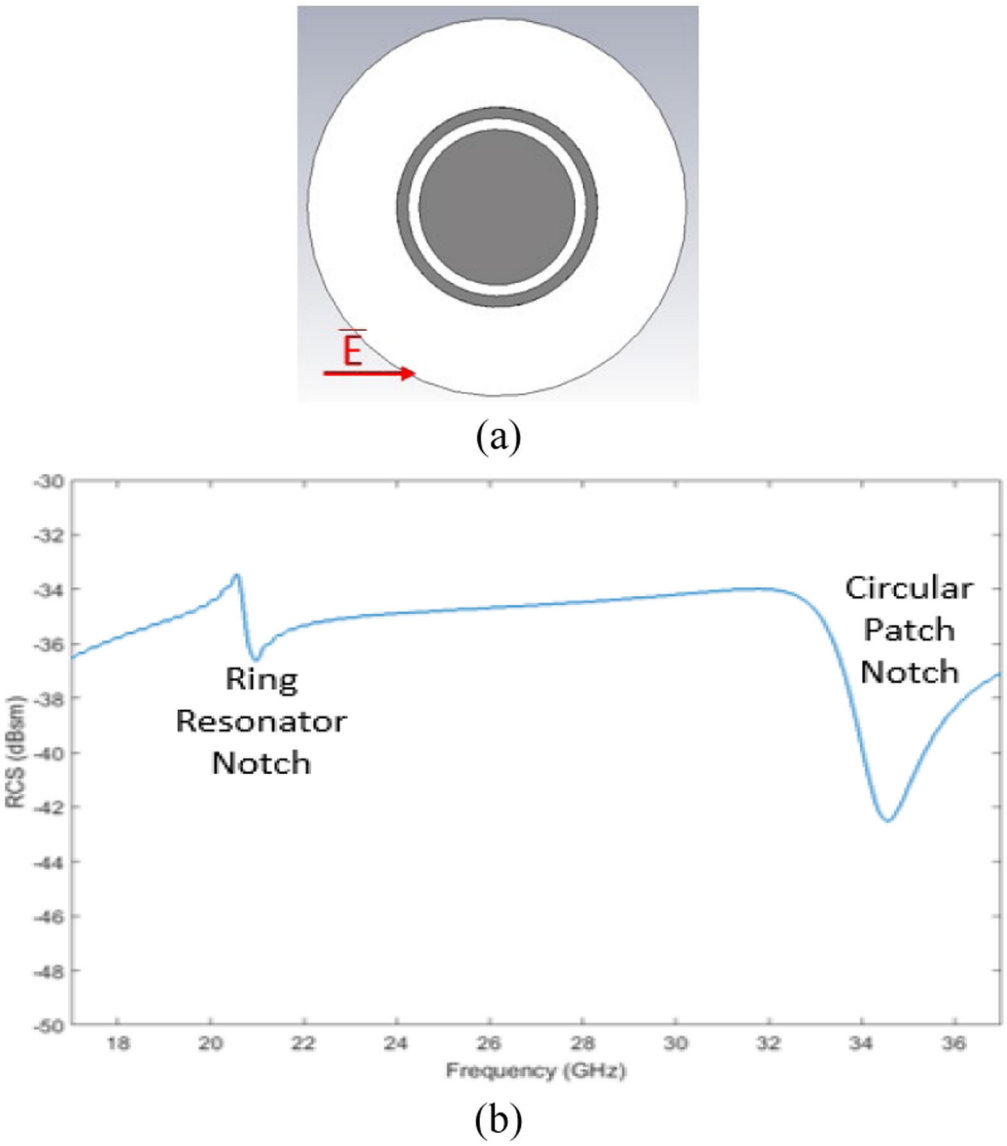

Fig. 2:

Basic Configuration of tag design and its RCS frequency response: a) CST Microwave Studio® model, b) RCS vs. frequency response.

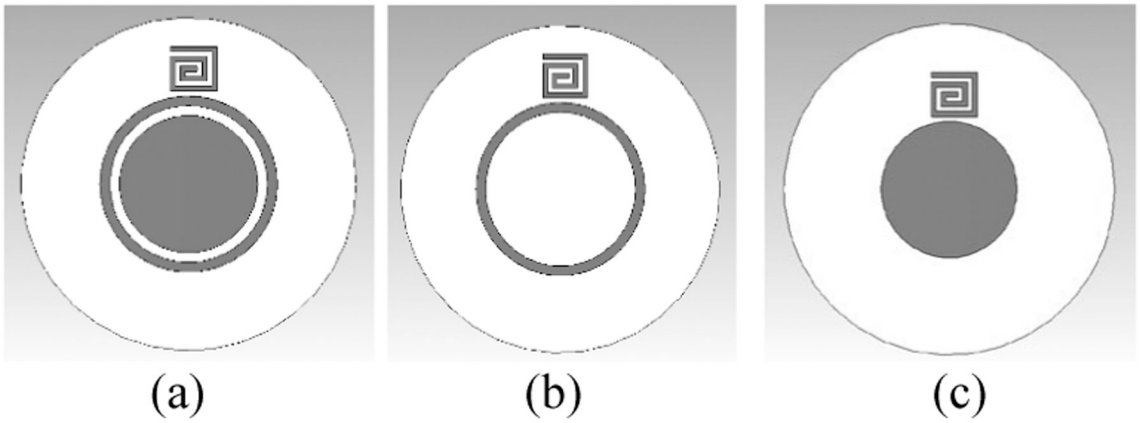

Fig. 3:

Tag configurations used in illustrating the necessity of the ring resonator element in this tag design: a) ring, patch, and spiral configuration, b) ring and spiral configuration, and c) patch and spiral configuration.

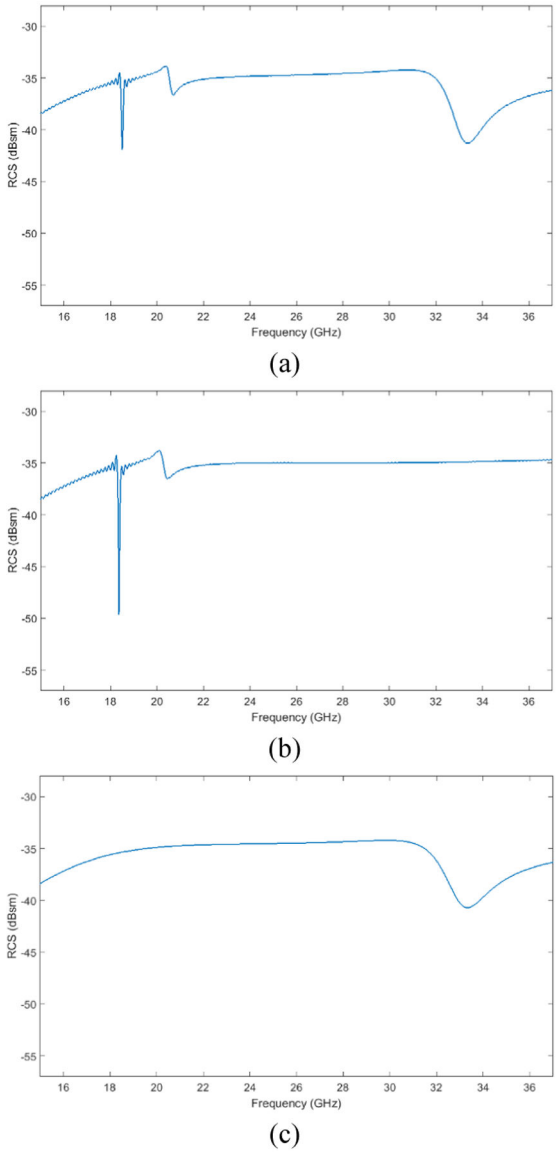

Fig. 4:

Responses of tags shown in Fig. 3: a) patch, ring, and spiral configuration RCS vs. frequency response, b) ring and spiral configuration RCS vs. frequency response, and c) patch and spiral configuration RCS vs. frequency response.

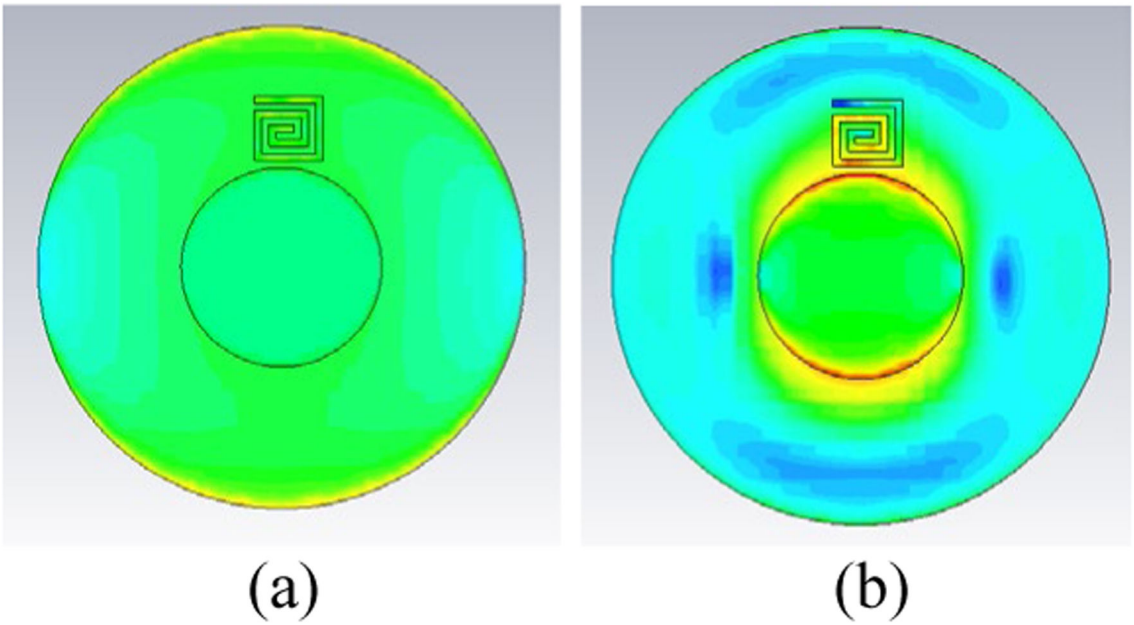

Fig. 5:
Surface current density simulation for configuration shown in Fig. 3c: a) surface current density at 18.5 GHz, and b) surface current density at 35 GHz.

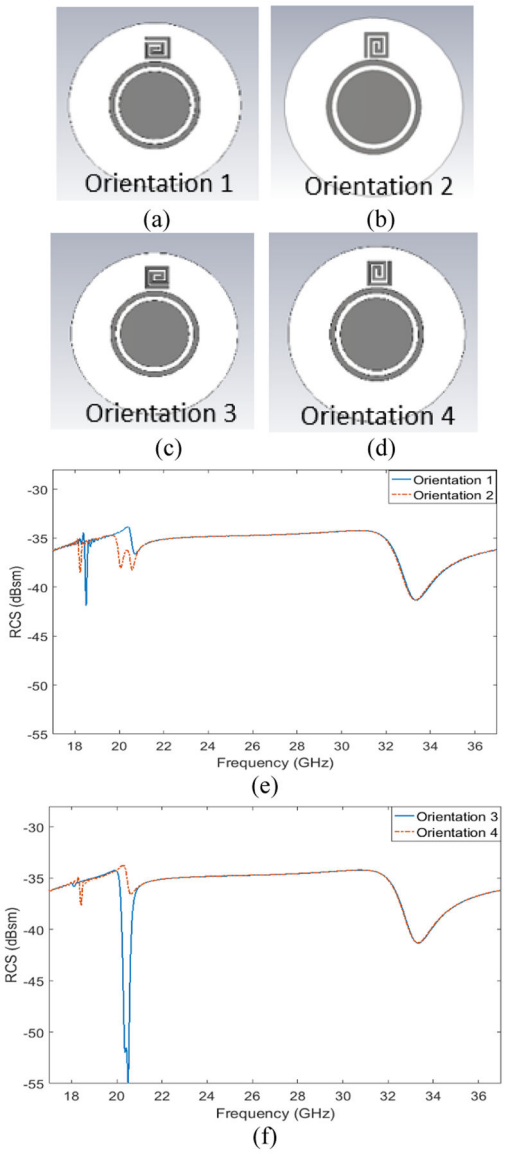

Fig. 6:

Tag response as a function of spiral orientation: a) orientation 1, b) orientation 2, c) orientation 3, d) orientation 4, e) Response for different spiral orientations 1 and 2, and f) Response for different spiral orientations 3 and 4.

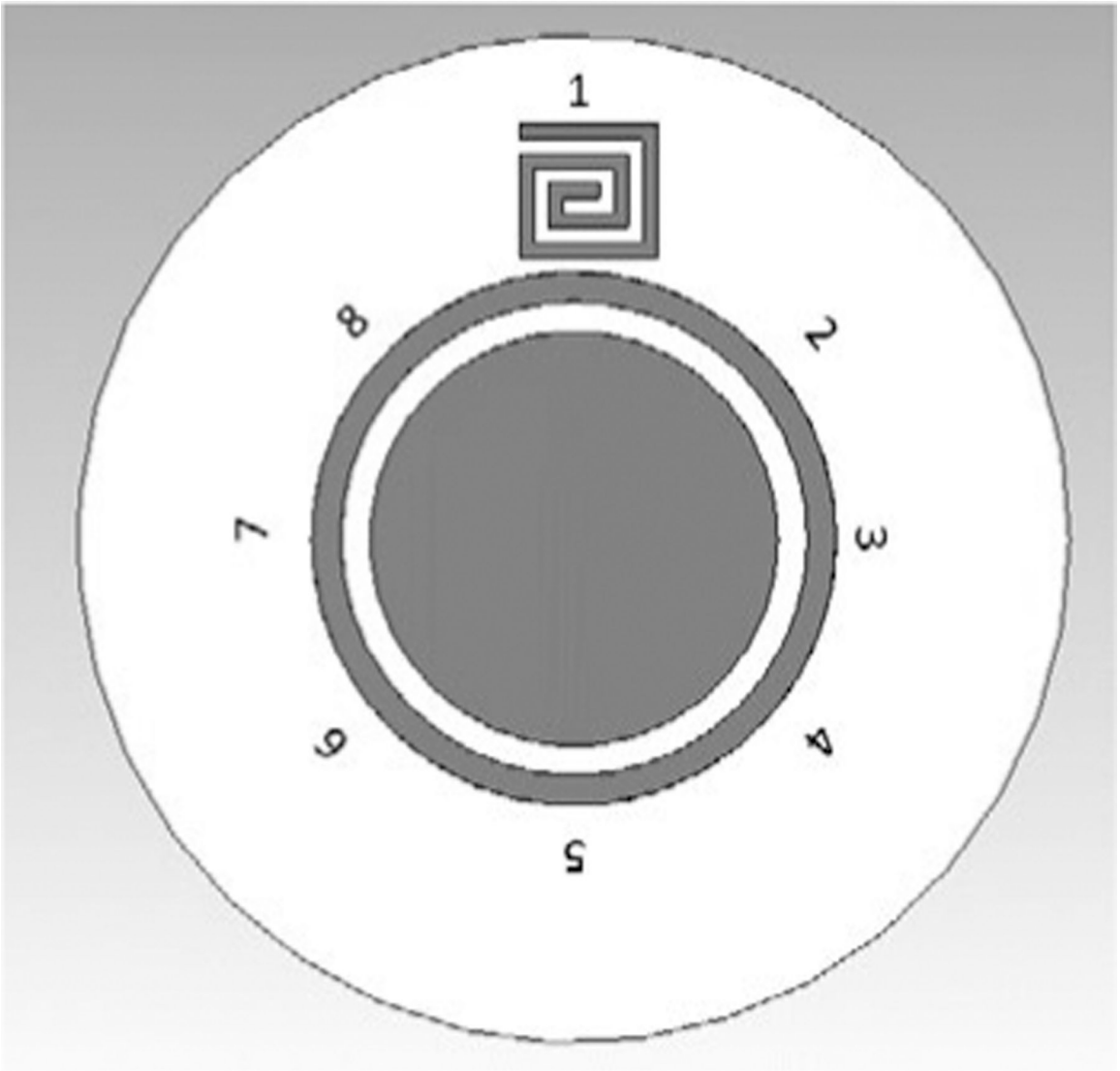

Fig. 7:
Spiral location designations.

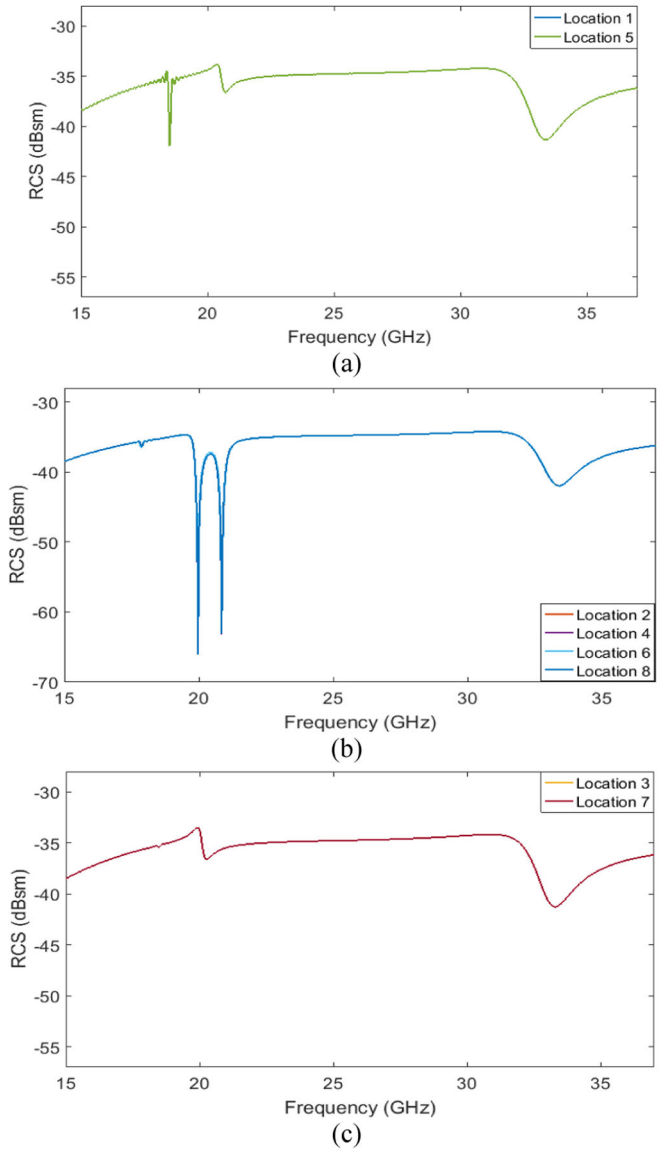

Fig. 8:

RCS vs. frequency response when the spiral is in different locations a) response for locations 1 and 5, b) response for locations 2, 4, 6, and 8, and c) response for locations 3 and 7.

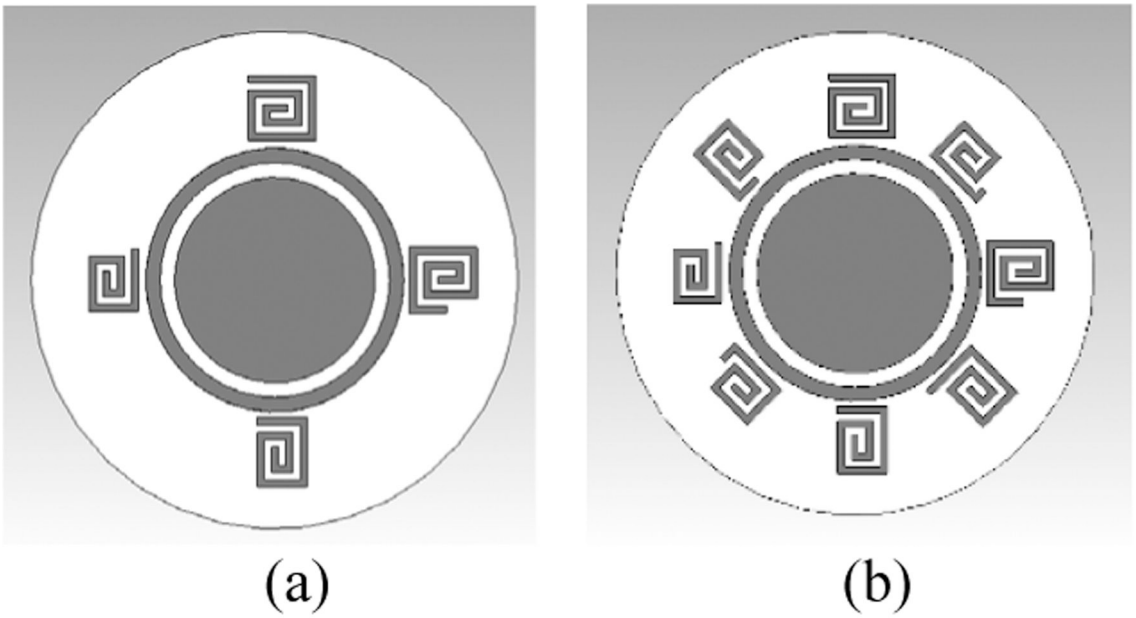

Fig. 9:
Tag models in CST Microwave Studio®: a) 4-spiral configuration, and b) 8-spiral configuration.

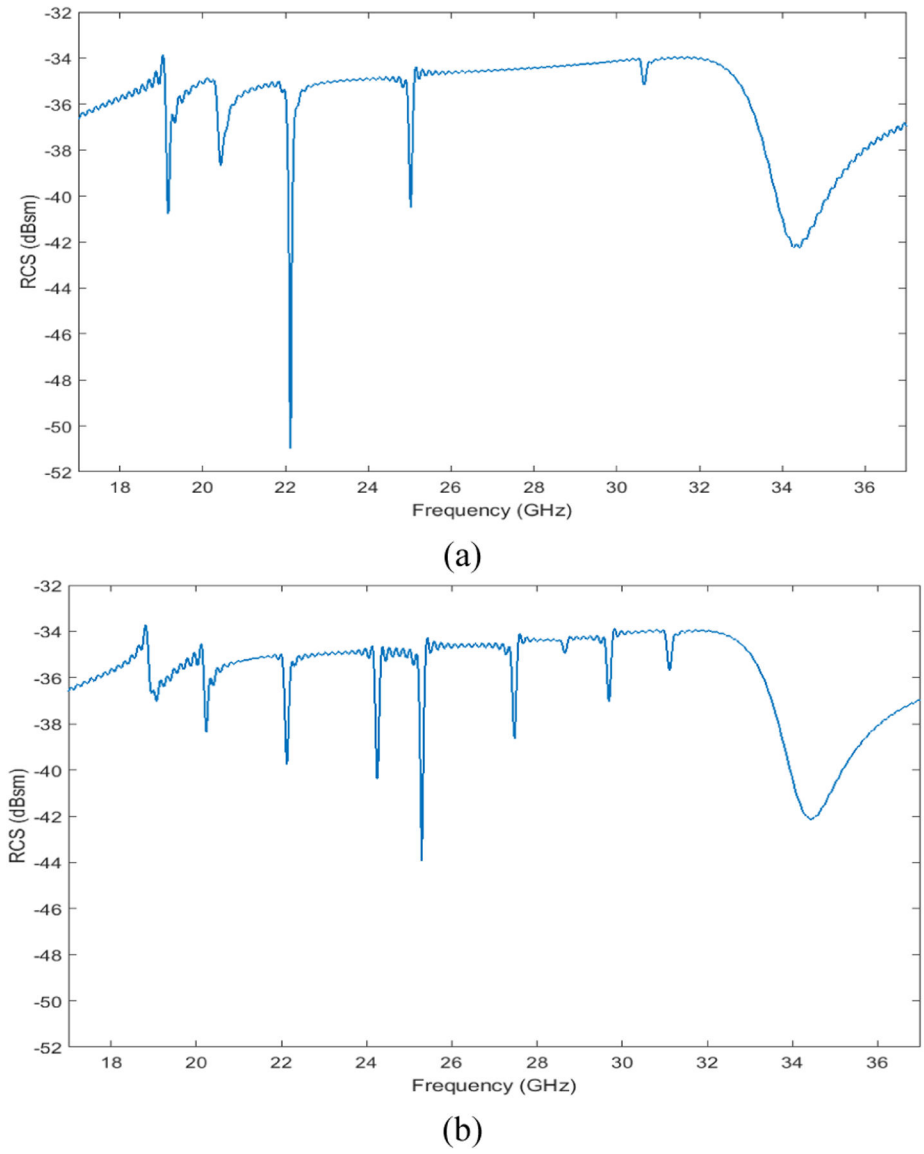

Fig.10:

RCS vs. frequency tag responses for two different tag configurations: a) 4-spiral tag response, and b) 8-spiral tag response.

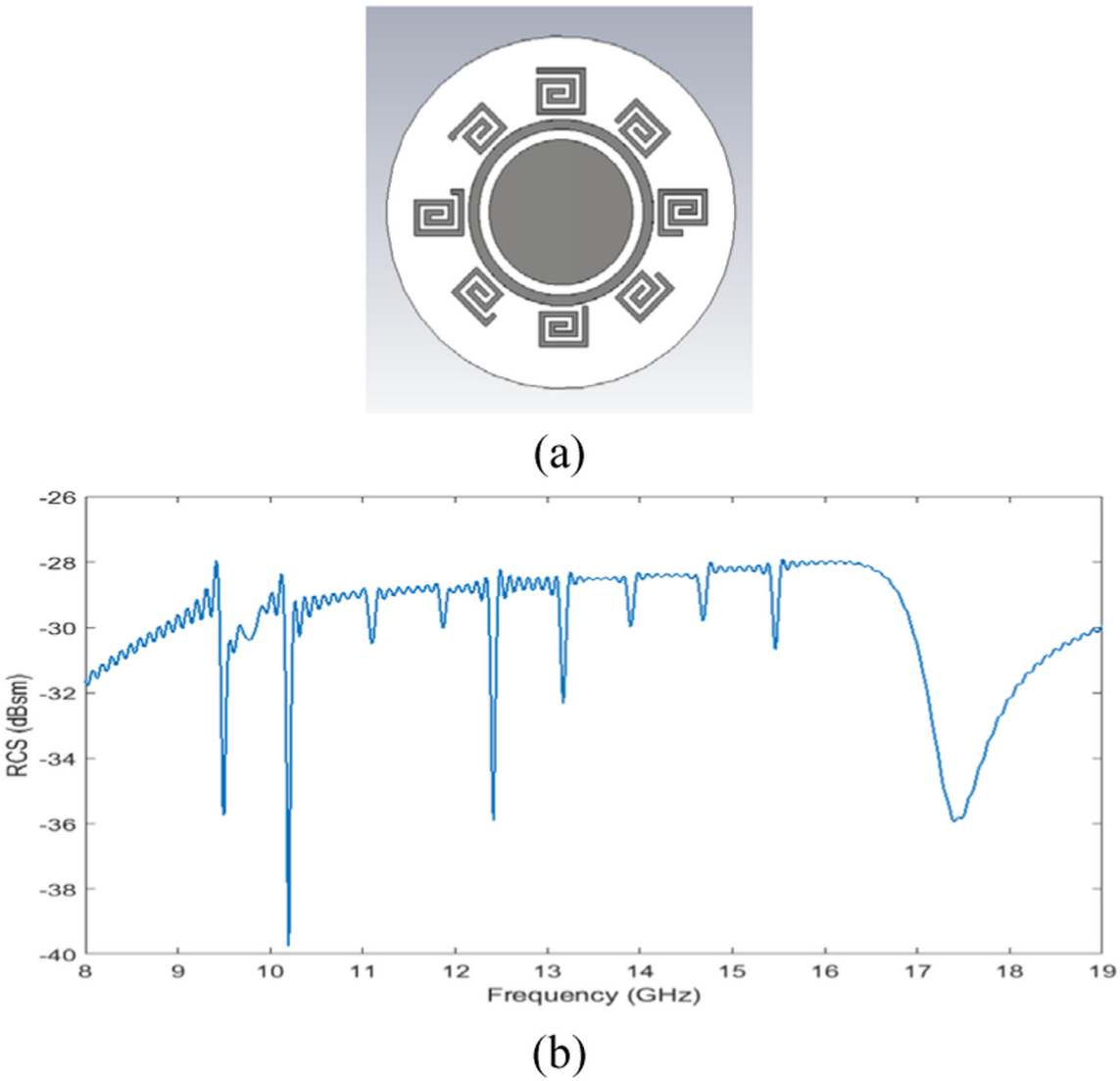

Fig. 11:
Lower frequency version of spiral tag: a) CST Microwave Studio® model of tag, and b) RCS vs. frequency response of tag.

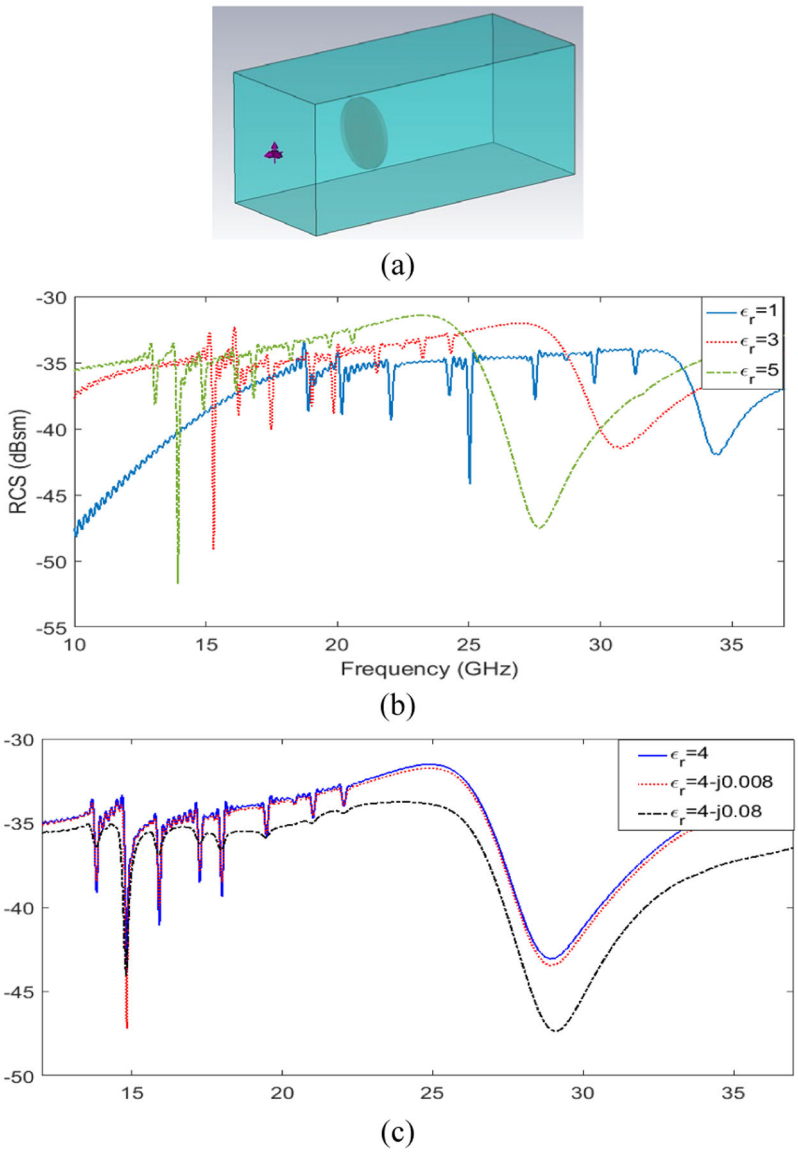

Fig. 12:

Tag as an embedded materials characterization sensor: a) simulation setup, b) effect of permittivity on response for three embedding materials, and c) effect of material loss on response for three embedding materials.

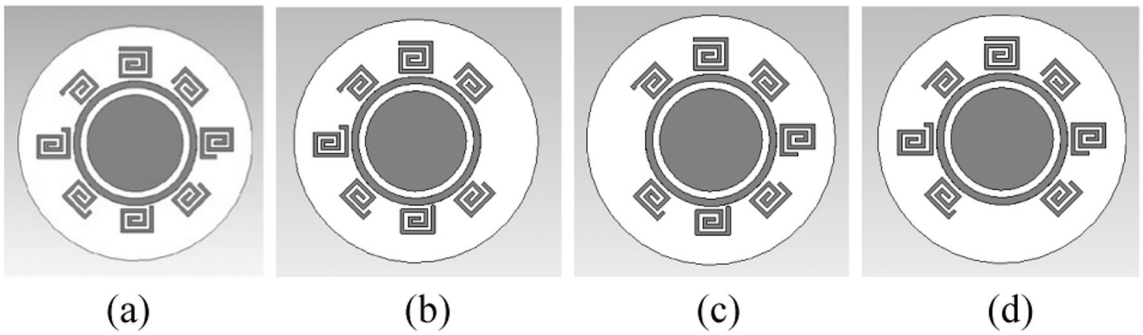

Fig. 13:
Test of ID application suitability: a) 8-spiral tag, b) tag with spiral 2 removed, c) tag with spiral 3 removed, and d) tag with spiral 4 removed.

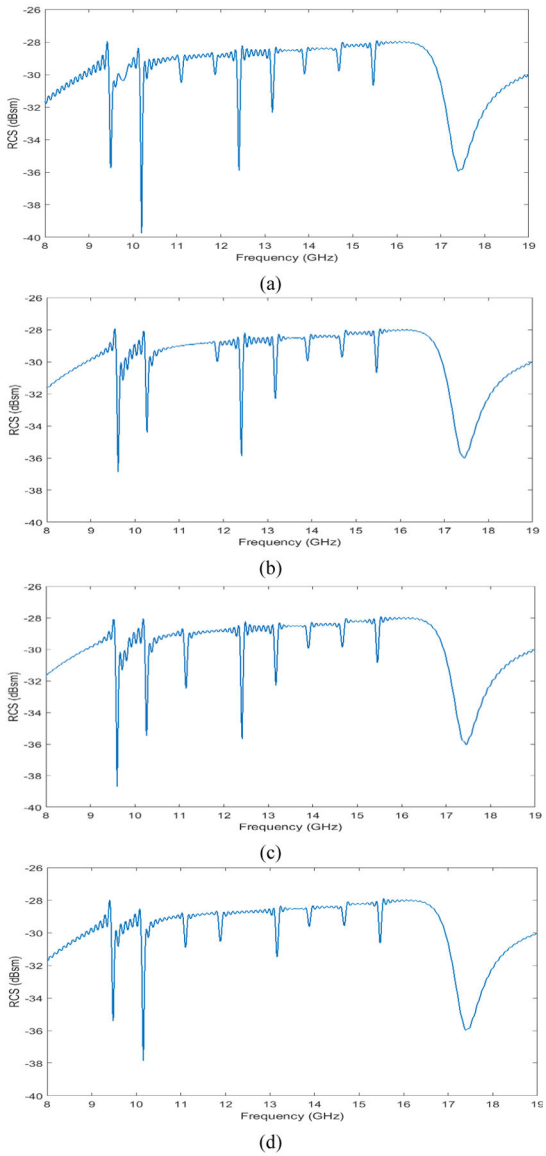

Fig. 14:

Frequency scaled 8-spiral tag for ID applications: a) Response for all spirals present, b) Response for tag when spiral 2 is removed, c) Response for tag when spiral 3 is removed, and d) Response when spiral 4 is removed.

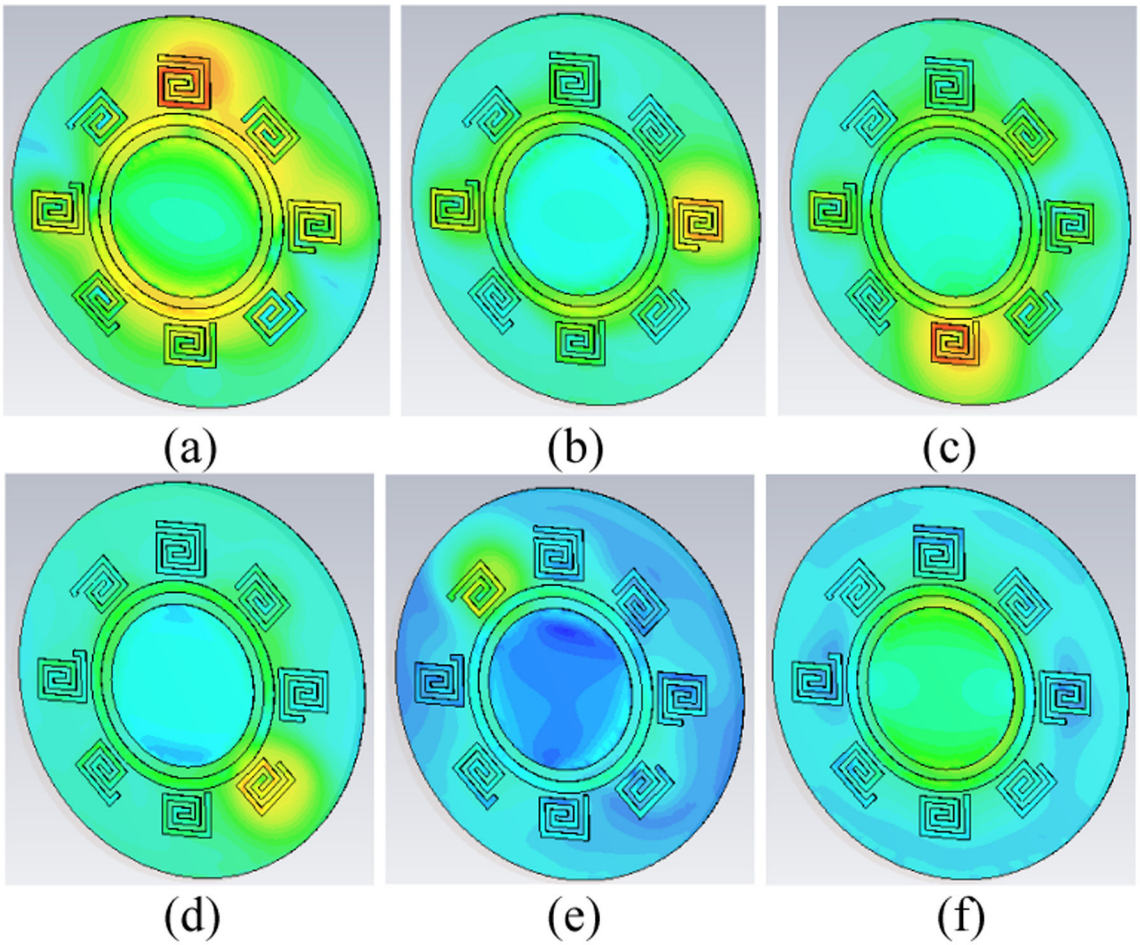

Fig. 15:

Surface current density simulation: a) 10.2 GHz surface current density, b) 11.1GHz surface current density, c) 12.4 GHz surface current density, d) 13.9 GHz surface current density, e) 15.5 GHz surface current density, and f) 17.4 GHz surface current density.

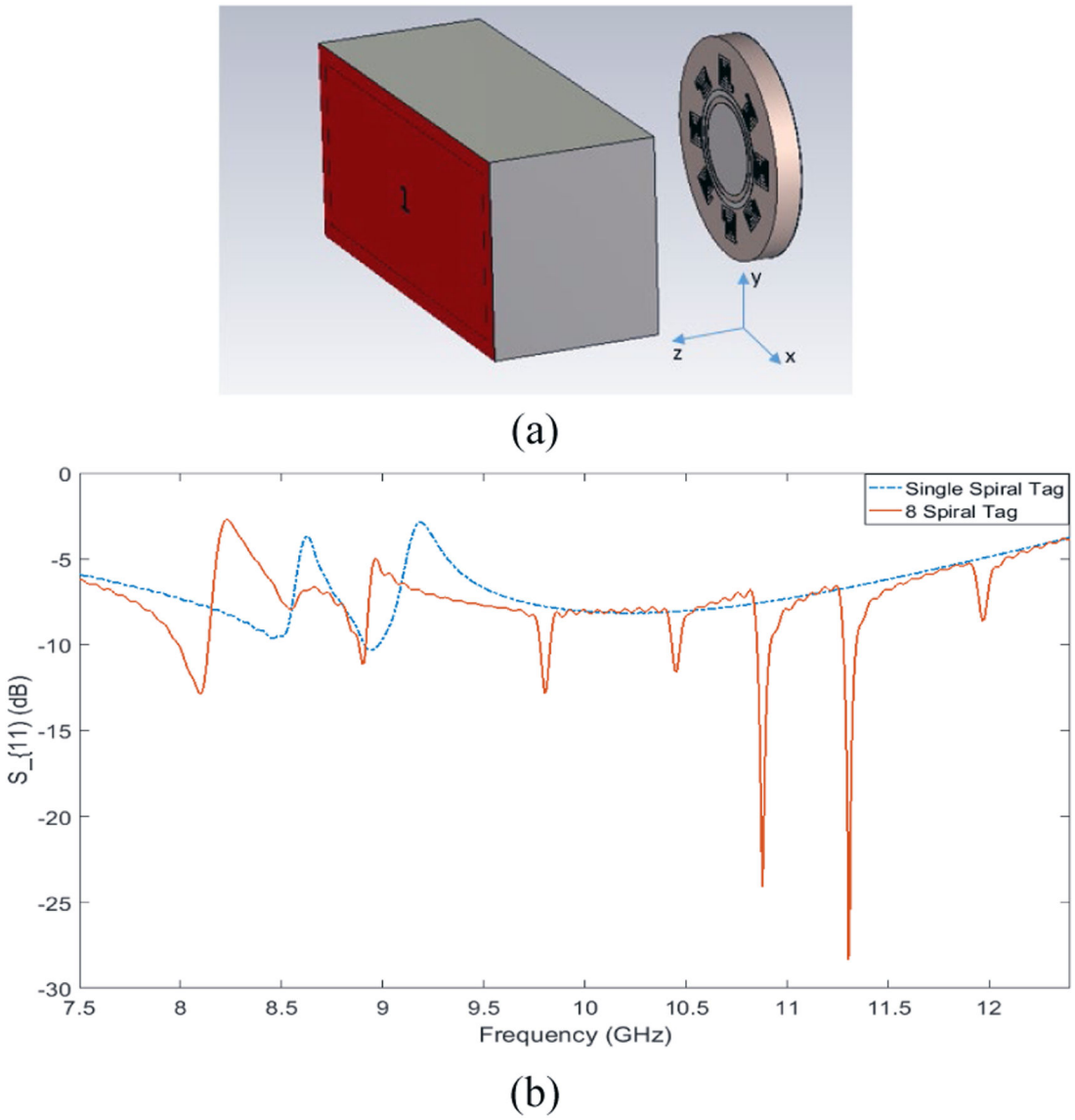

Fig. 16:

Simulated S_{11} responses of 8-spiral and single spiral fabricated tags: a) simulation setup, and b) simulated S_{11} for the two tags shown in Fig. 17.

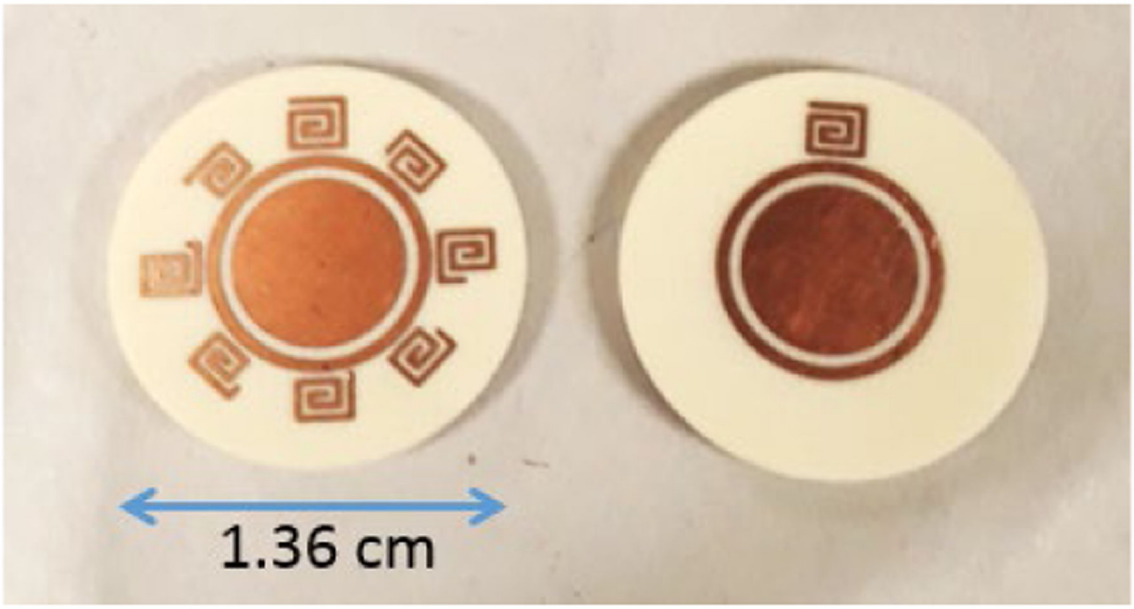

Fig. 17:
Manufactured tags.

Fig. 18:
Measurement setup.

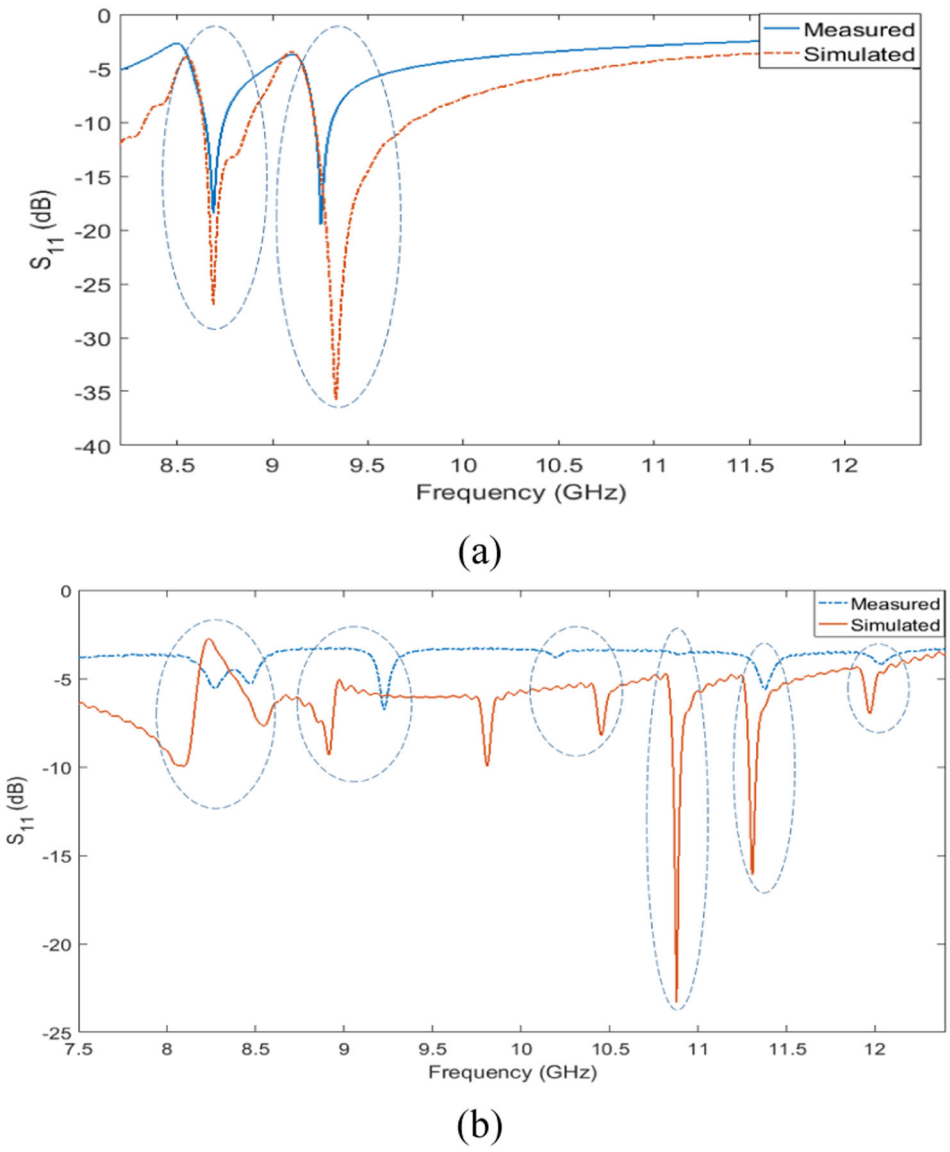

Fig. 19:

Measurement results in comparison to simulated results: a) single spiral tag simulated and measured S_{11}, and b) 8-spiral tag simulated and measured S_{11}.

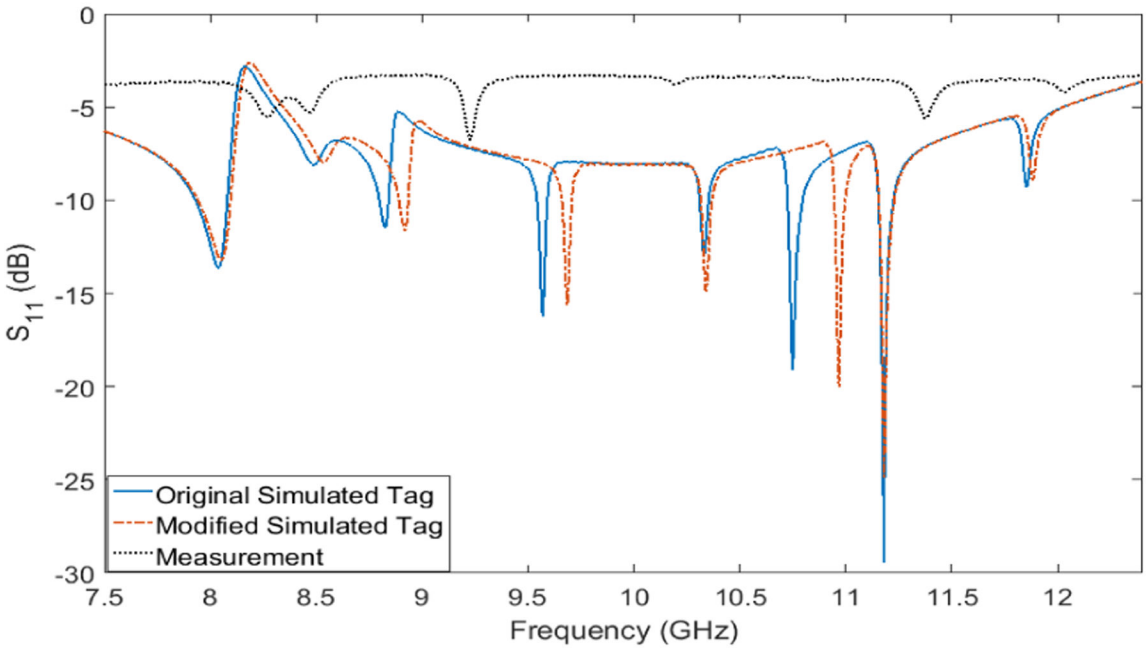

Fig. 20:

Simulation vs. measurement results showing the effect of modifying three spiral lengths on the S_{11} response.

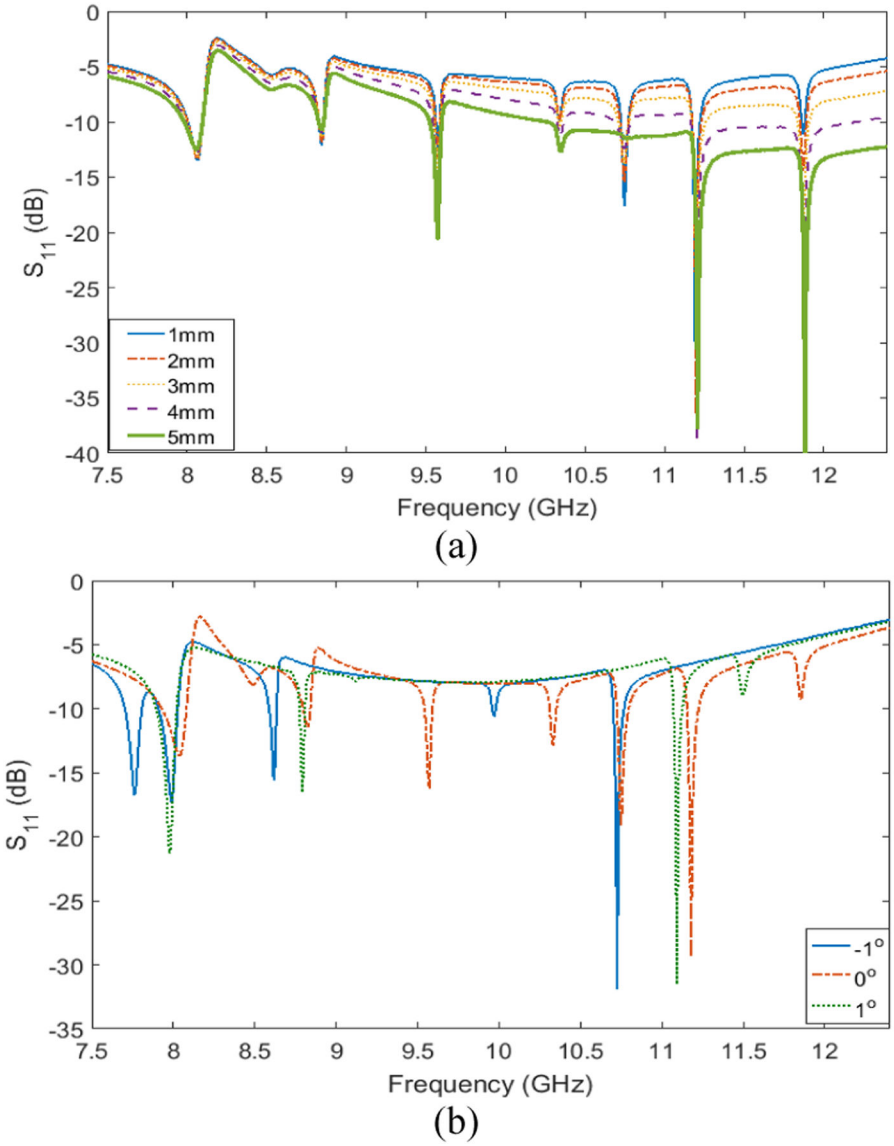

Fig. 21:

Illustration of effect of misalignment on tag response: a) Effect of translation along x-axis, and b) Effect of rotation about x-axis.

TABLE I

8-Spiral tag metrics for different coding methods

Coding Method	Bit Density (bits/cm^2) for Version 1	Bit Density (bits/cm^2) for Version 2
1	27.54	6.88
2	27.54	6.88
3	55.07	16.52
4	55.07	16.52
5	344.19	175.54

TABLE II

Bit Density for Backscatter-based tags

Resonator Type	Coding Method	Bit Density (bits/cm^2)	Reference
C-Shaped	6	2.86	[46]
Circular Slot	2	4.19	[12]
Square	2	0.56	[47]
C-Shaped	4	28.57	[48]
Square Loops	4	19	[38]
Bow-tie with slots	2	5.76	[49]
Spiral-loaded Dipoles	2	0.7	[50]
Dual-polarized slot	2	9.03	[51]